

SUPPORTING INFORMATION

Conductance Behavior of Tetraphenyl-aza-BODIPYs

Andrei Markin^{a,‡}, Ali K. Ismael,^{b,c,‡*} Ross J. Davidson,^{a*} David C. Milan,^{d,‡} Richard J. Nichols,^{d*} Simon J. Higgins,^d Colin J. Lambert,^b Yu-Ting Hsu,^a Dmitry S. Yufit,^a Andrew Beeby,^{a*}.

^a*Department of Chemistry, Durham University, South Rd, Durham, DH1 3LE, UK*

^b*Department of Physics, University of Lancaster, Lancaster LA1 4YB, U.K.*

^c*Department of Physics, College of Education for Pure Science, Tikrit University, Tikrit, Iraq*

^d*Department of Chemistry, University of Liverpool, Crown St, Liverpool, L69 7ZD, UK*

[‡]*These Authors contributed equally to this work*

Table of Contents

a) Experimental

- 1. Synthesis S3
- 2. NMR spectra of reported compounds S13
- 3. Crystallographic data S24

b) Photophysical Measurements

- 1. PLQY S36
- 2. Solvatochromism S40
- 3. Computational S43

c) Conductance measurements

- 1. Conductance 1D and 2D Histograms S45

d) Theoretical details

- 1. Geometry of isolated molecules and their junctions S49
- 2. Binding energy of 12 on gold via two different anchor groups S51
- 3. Do 11 and 13 π -stack onto gold? S53
- 4. Wave function plots for 11, 12 and 13 S55
- 5. HOMO-LUMO gap S58
- 6. Transmission coefficient S59
- 7. Comparison with experimental measurements S61
- 8. Breaking off distance S62
- 9. Discussion of alternative binding motifs S62
- 10. Tight binding model S62

e) References

S64

a) Experimental

Instrumentation. NMR spectra were recorded in deuterated solvent solutions on a Varian VNMRS-700 spectrometer and referenced against solvent resonances (^1H , ^{13}C). ASAP data were recorded on a Xevo QTOF (Waters) high resolution, accurate mass tandem mass spectrometer equipped with Atmospheric Pressure Gas Chromatography (APGC) and Atmospheric Solids Analysis Probe (ASAP). MALDI data were recorded on a Bruker Autoflex II ToF/FoF spectrometer. Microanalyses were performed by Elemental Analysis Service, London Metropolitan University, UK or Elemental Microanalysis service, Durham University, UK.

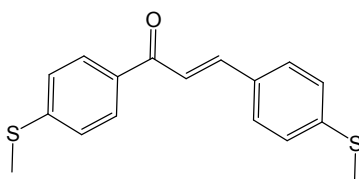
General details. The compounds 3-(4-(methylthio)phenyl)-1-phenylprop-2-en-1-one (**2**)¹ and (4-ethynylphenyl)(methyl)sulfane² were prepared according to published methods, all other chemicals were sourced from standard chemical suppliers.

1. Synthesis.

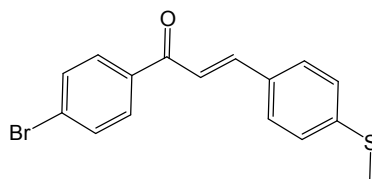
General procedure for synthesis of chalcones (1, 3). 4-(methylthio)benzaldehyde (13.2 mL, 15.2 g, 100 mmol) was added to NaOH (4.68 g, 117 mmol) in 50% aqueous ethanol (250 mL). The respective aryl ketone (100 mL) was added to the previous solution over approximately 10 minutes with vigorous stirring. After another 10 minutes, the resulting precipitate was filtered and washed with aqueous ethanol. The product was purified by recrystallisation from methanol and dried in vacuo.

1,3-bis(4-(methylthio)phenyl)prop-2-en-1-one (1): The aryl ketone 1-(4-(methylthio)phenyl)ethanone (23.0 g, 138 mmol) was used, yielding a yellow solid. **Yield:** 29.84g (85%). **$^1\text{H NMR}$** (700 MHz; CDCl_3): δ_{H} 7.94 (2H, d, $J_{\text{HH}} = 8.3$ Hz, H_{10}), 7.76 (1H, d,

$J^{\beta}_{\text{HH}} = 15.6$ Hz, H₆), 7.54 (2H, d, $J^{\beta}_{\text{HH}} = 8.3$ Hz, H₄), 7.46 (1H, d, $J^{\beta}_{\text{HH}} = 15.6$ Hz, H₇), 7.30 (2H, d, $J^{\beta}_{\text{HH}} = 8.4$ Hz, H₁₁), 7.24 (2H, d, $J^{\beta}_{\text{HH}} = 8.3$ Hz, H₃), 2.53 (3H, s, H₁₃), 2.51 (3H, s, H₁) ppm. $^{13}\text{C}\{^1\text{H}\}$ NMR (176 MHz; CDCl₃): δ_{C} 189.2 (C₈), 145.6 (C₁₂), 144.1 (C₆), 142.4 (C₂), 134.7 (C₉), 131.6 (C₅), 129.0 (C₁₀), 128.9 (C₄), 126.1 (C₃), 125.0 (C₁₁), 120.8 (C₇), 15.3 (C₁), 14.9 (C₁₃) ppm. **MS**(ASAP⁺): m/z 301.050 [M+H]⁺. **Acc-MS**(ASAP⁺): m/z 301.07235 [M+H]⁺ calcd. for C₁₇H₁₇OS₂ m/z 301.0721 ($|\Delta m/z| = 4.7$ ppm). **Anal. Clac.** for C₁₇H₁₆OS₂: C, 67.96; H, 5.37; N, 0.00 %. **Found:** C, 67.60; H, 5.32; N, -0.03 %.

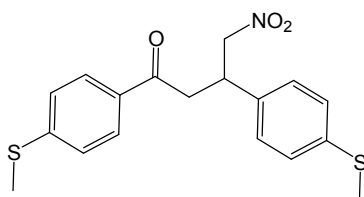


(4-bromophenyl)-3-(4-(methylthio)phenyl)prop-2-en-1-one (3): The aryl ketone 1-(4-bromophenyl)ethan-1-one (23.04 g, 117 mmol) was used, yielding a yellow powder. **Yield:** 35.20 g (90%). ^1H NMR (700 MHz; CDCl₃): δ_{H} 7.87 (2H, d, $J^{\beta}_{\text{HH}} = 8.4$ Hz, H₁₀), 7.76 (1H, d, $J^{\beta}_{\text{HH}} = 15.8$ Hz, H₆), 7.63 (2H, d, $J^{\beta}_{\text{HH}} = 8.4$ Hz, H₁₁), 7.54 (2H, d, $J^{\beta}_{\text{HH}} = 7.9$ Hz, H₃), 7.41 (1H, d, $J^{\beta}_{\text{HH}} = 15.8$ Hz, H₇), 7.25 (2H, d, $J^{\beta}_{\text{HH}} = 8.2$ Hz, H₄), 2.51 (3H, s, H₁) ppm. $^{13}\text{C}\{^1\text{H}\}$ NMR (176 MHz; CDCl₃): δ_{C} 189.2 (C₈), 144.8 (C₆), 142.7 (C₂), 137.0 (C₁₂), 131.8 (C₁₁), 131.1 (C₅), 129.9 (C₁₀), 128.8 (C₃), 127.7 (C₉), 125.9 (C₄), 120.3 (C₇), 15.0 (C₁) ppm. **MS**(ASAP⁺): m/z 333.174 [M+H]⁺. **Acc-MS**(ASAP⁺): m/z 332.9944 [M+H]⁺ calcd. for C₁₆H₁₄OSBr m/z 332.9949 ($|\Delta m/z| = 1.5$ ppm). **Anal. Clac.** for C₁₆H₁₃OSBr: C, 57.67; H, 3.93; N, 0.00 %. **Found:** C, 57.61; H, 3.93; N, -0.07 %.



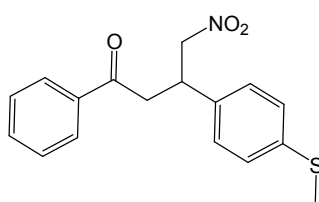
General procedure for synthesis of compounds (4-6). The respective chalcone (**1-3**) was dissolved in methanol, then nitromethane (4 mL, 75 mmol) and diethylamine (7.7 ml, 75.0 mmol) were added, and the mixture was heated under reflux for 16 h. After which, formation of a precipitate was observed, the mixture was acidified and the product extracted with DCM, followed by filtration with activated charcoal. The solvent was removed in vacuo to yield the respective product.

1,3-bis(4-(methylthio)phenyl)-4-nitrobutan-1-one (4): The starting material was **1** (5 g, 16.7 mmol), yielding a pale-yellow solid. **Yield:** 2.90g (53%). **¹H NMR** (700 MHz; CDCl₃): δ_H 7.81 (2H, d, $J_{\text{HH}} = 8.6$ Hz, H₁₀), 7.25 (2H, d, $J_{\text{HH}} = 8.6$ Hz, H₁₁), 7.20 (4H, m, H₃+H₄), 4.80 (1H, dd, $J_{\text{HH}} = 12.5$ Hz, $J_{\text{HH}} = 6.6$ Hz, H₁₄), 4.65 (1H, dd, $J_{\text{HH}} = 12.5$ Hz, $J_{\text{HH}} = 8.1$ Hz, H_{14'}), 4.17 (1H, m, H₆), 3.37 (2H, m, H₇), 2.51 (3H, s, H₁₃), 2.45 (3H, s, H₁) ppm. **¹³C{¹H} NMR** (176 MHz; CDCl₃): δ_C 195.8 (C₈), 146.8 (C₁₂), 138.3 (C₂), 135.9 (C₅), 132.7 (C₉), 128.5 (C₁₀), 128.05 (C₃/C₄), 127.1 (C₃/C₄), 125.1 (C₁₁), 79.6 (C₁₄), 41.3 (C₇), 39.0 (C₆), 15.8 (C₁), 14.8 (C₁₃) ppm. **MS(ASAP⁺):** m/z 362.079 [M+H]⁺. **Acc-MS(ASAP⁺):** m/z 362.0881 [M+H]⁺ calcd. for C₁₈H₂₀NO₃S₂ m/z 362.0885 ($|\Delta m/z| = 1.1$ ppm). **Anal. Clac.** for C₁₈H₁₉NO₃S₂: C, 59.81; H, 5.30; N, 3.87 %. **Found:** C, 59.51; H, 5.24; N, 3.74 %.

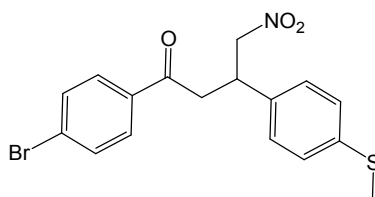


3-(4-(methylthio)phenyl)-4-nitro-1-phenylbutan-1-one (5): The starting material was **2** (5 g, 19.7 mmol), yielding a pale-yellow solid. **Yield:** 3.84 g (62%). **¹H NMR** (700 MHz; CDCl₃): δ_H 7.97 (2H, d, $J_{\text{HH}} = 9.5$ Hz, H₁₀), 7.63 (1H, t, $J_{\text{HHH}} = 7.4$ Hz, H₁₂), 7.51 (2H, t, $J_{\text{HHH}} = 7.8$

Hz, H₁₁), 7.26 (4H, m, H₃+H₄), 4.86 (1H, dd, $J_{\text{HH}}^{\beta} = 12.6$ Hz, $J_{\text{HH}}^{\alpha} = 6.6$ Hz, H₁₃), 4.72 (1H, dd, $J_{\text{HH}}^{\beta} = 12.5$ Hz, $J_{\text{HH}}^{\alpha} = 8.1$ Hz, H_{13'}), 4.25 (1H, m, H₆), 3.50 (2H, m, H₇), 2.51 (3H, s, H₁) ppm. $^{13}\text{C}\{^1\text{H}\}$ NMR (176 MHz; CDCl₃): δ_{C} 196.8 (C₈), 138.3 (C₂), 136.4 (C₉), 135.9 (C₅), 133.2 (C₁₁), 133.5 (C₁₂), 128.1 (C₁₀), 128.0 (C₄), 127.1 (C₃), 79.6 (C₁₃), 41.5 (C₇), 38.9 (C₆), 15.8 (C₁) ppm. MS(ASAP⁺): m/z 316.097 [M+H]⁺. Acc-MS(ASAP⁺): m/z 316.0988 [M+H]⁺ calcd. for C₁₇H₁₈NO₃S m/z 316.1007 ($|\Delta m/z| = 6.0$ ppm). Anal. Clac. for C₁₇H₁₇NO₃S: C, 64.74; H, 5.43; N, 4.44 %. Found: C, 64.45; H, 5.36; N, 4.07 %.

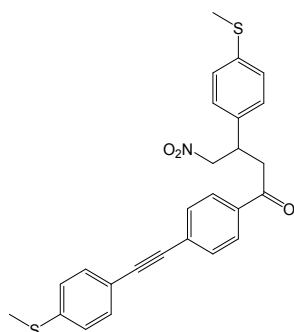


1-(4-bromophenyl)-3-(4-(methylthio)phenyl)-4-nitrobutan-1-one (6): The starting material was **3** (5 g, 15.0 mmol), yielding a pale-yellow solid. Yield: 5.32g (90%). ^1H NMR (700 MHz; CDCl₃): δ_{H} 7.72 (2H, d, $J_{\text{HH}}^{\beta} = 8.6$ Hz, H₁₀), 7.54 (2H, d, $J_{\text{HH}}^{\beta} = 8.6$ Hz, H₁₁), 7.16 (4H, m, H₃), 4.76 (1H, dd, $J_{\text{HH}}^{\beta} = 12.6$ Hz, $J_{\text{HH}}^{\alpha} = 6.6$ Hz, H₁₃), 4.63 (1H, dd, $J_{\text{HH}}^{\beta} = 12.6$ Hz, $J_{\text{HH}}^{\alpha} = 8.1$ Hz, H_{13'}), 4.14 (1H, dq, $J_{\text{HH}}^{\beta} = 8.0$ Hz, $J_{\text{HH}}^{\alpha} = 6.8$ Hz, H₆), 3.36 (2H, m, H₇), 2.40 (3H, s, H₁) ppm. $^{13}\text{C}\{^1\text{H}\}$ NMR (176 MHz; CDCl₃): δ_{C} 195.8 (C₈), 138.1 (C₂), 135.5 (C₄), 135.0 (C₁₂), 132.2 (C₁₁), 129.5 (C₁₀), 128.7 (C₉), 127.2 (C₅), 126.8 (C₃), 79.4 (C₁₃), 41.3 (C₇), 38.7 (C₆), 15.5 (C₁) ppm. MS(ASAP⁺): m/z 394.992 [M+H]⁺ (25%), 346.989 [M-NO₂]⁺ (100%). Acc-MS(ASAP⁺): m/z 394.0104 [M+H]⁺ calcd. for C₁₇H₁₇NO₃SBr m/z 316.1007 ($|\Delta m/z| = 2.3$ ppm). Anal. Clac. for C₁₇H₁₆NO₃SBr: C, 51.79; H, 4.09; N, 3.55 %. Found: C, 52.08; H, 4.07; N, 3.37 %.



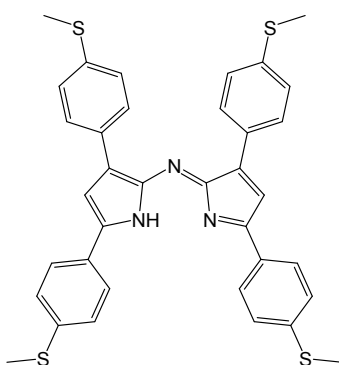
3-(4-(methylthio)phenyl)-1-(4-((4-(methylthio)phenyl)ethynyl)phenyl)-4-nitrobutan-1-one

(7): In a nitrogen atmosphere, **6** (5.05 g, 12.8 mmol), CuI (243 mg, 1.28 mmol), PdCl₂(PPh₃)₂ (896 mg, 1.28 mmol) and 4-ethynylthioanisole (1.90 g, 12.8 mmol) were dissolved in THF (50 mL). The resulting solution was degassed via three freeze-pump-thaw cycles, before the addition of Et₃N (5 mL). The mixture was left to reflux for 16 h, the solution was then cooled, and the solvent removed under *vacuo*. The residue was purified by column chromatography on silica gel eluted with 4:1 DCM:hexane. Recrystallisation from methanol yielded a pure product as a yellow solid. **Yield:** (3.44 g, 58%). **¹H NMR** (700 MHz; CDCl₃): δ_H 7.87 (2H, d, *J*_{HH} = 8.6 Hz, H₁₁), 7.57 (2H, d, *J*_{HH} = 8.6 Hz, H₁₂), 7.44 (2H, d, *J*_{HH} = 8.6 Hz, H₄), 7.23-7.19 (6H, m, H₃+H₁₇+H₁₈), 4.81 (1H, dd, *J*_{HH} = 12.6 Hz, *J*_{HH} = 6.7 Hz, H₈), 4.66 (1H, dd, *J*_{HH} = 12.6 Hz, *J*_{HH} = 8.0 Hz, H₈), 4.18 (1H, p, *J*_{HH} = 7.0 Hz, H₆), 3.41 (2H, m, H₇), 2.50 (3H, s, H₁), 2.46 (3H, s, H₂₀) ppm. **¹³C{¹H} NMR** (176 MHz; CDCl₃): δ_C 196.0 (C₉), 140.5 (C₂), 138.4 (C₁₉), 135.8 (C₅), 135.3 (C₁₃), 132.1 (C₄), 131.8 (C₁₂), 128.9 (C₁₀), 128.1 (C₁₁), 128.0 (C₃), 127.2 (C₁₆/C₁₇/C₁₈), 125.9 (C₁₆/C₁₇/C₁₈), 118.7 (C₁₆/C₁₇/C₁₈), 93.3 (C₁₄), 88.7 (C₁₅), 79.6 (C₈), 41.6 (C₇), 38.9 (C₆), 15.8 (C₂₀), 15.4 (C₁) ppm. **MS(ASAP⁺):** *m/z* 462.120 [M+H]⁺ (50%), 401.107 [M-CH₂NO₂]⁺ (100%). **Acc-MS(ASAP⁺):** *m/z* 462.1187 [M+H]⁺ calcd. for C₂₆H₂₄NO₃S₂ *m/z* 462.1198 (|Δ*m/z*| = 2.4 ppm). **Anal. Clac.** for C₂₆H₂₃NO₃S₂: C, 67.65; H, 5.02; N, 3.03 %. **Found:** C, 66.85; H, 4.93; N, 2.81 %.

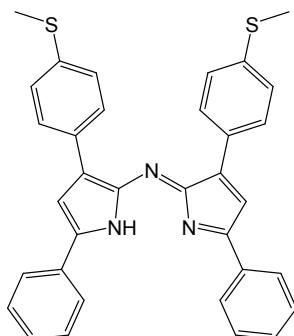


General procedure for synthesis of aza-DIPY's (8-10). Respective compounds (**4**, **5**, and **7**) and ammonium acetate (10 eq) were dissolved in n-butanol and the yellow solution was heated under reflux for 24 h, during which precipitate formation was observed, with the color changing to dark blue/green, then to dark purple. The crude product was collected as a precipitate via filtration, purification was achieved by Soxhlet extraction using ethanol to remove impurities, followed by DCM to extract the product.

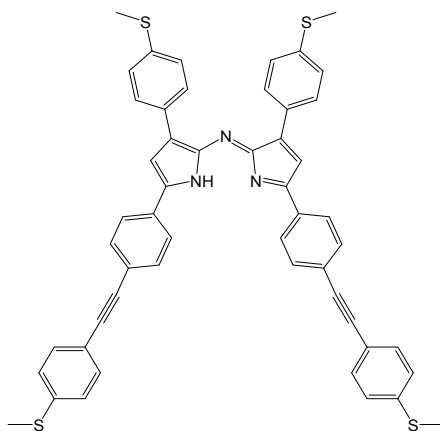
***N*-(3,5-bis(4-(methylthio)phenyl)-1*H*-pyrrol-2-yl)-3,5-bis(4-(methylthio)phenyl)-2*H*-pyrrol-2-imine (**8**):** The starting material was **4** (2.90 g, 1.03 mmol) to give a dark purple solid. **Yield:** 0.14 g (6%). **MS(MALDI):** m/z 632.9 $[M]^+$. **Anal. Clac.** for $C_{36}H_{31}N_3S_4 \cdot H_2O$: C, 66.33; H, 5.10; N, 6.45 %. **Found:** C, 66.26; H, 4.83; N, 6.68 %.



***3*-(4-(methylthio)phenyl)-*N*-(3-(4-(methylthio)phenyl)-5-phenyl-1*H*-pyrrol-2-yl)-5-phenyl-2*H*-pyrrol-2-imine (**9**):** The starting material was **5** (3.80 g, 12.06 mmol) to give a dark purple solid. **Yield:** 1.20 g (37%). **MS(MALDI):** m/z 540.9 $[M]^+$. **Anal. Clac.** for $C_{34}H_{27}N_3S_2 \cdot \frac{1}{2} H_2O$: C, 74.15; H, 5.12; N, 7.63 %. **Found:** C, 74.22; H, 4.96; N, 7.38 %.



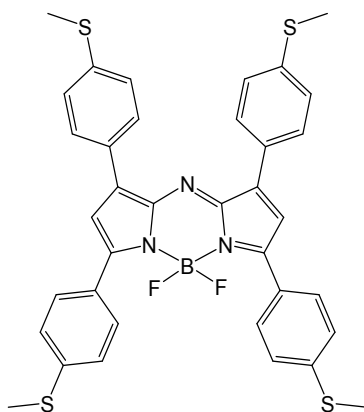
3-(4-(methylthio)phenyl)-N-(3-(4-(methylthio)phenyl)-5-(4-((4-(methylthio)phenyl)ethynyl)phenyl)-1H-pyrrol-2-yl)-5-(4-((4-(methylthio)phenyl)ethynyl)phenyl)-2H-pyrrol-2-imine (10): The starting material was **7** (1.50 g, 3.25 mmol), and the general procedure was followed with one alteration; upon the final Soxhlet extraction with DCM, the precipitate was collected to give a dark purple powder. **Yield:** 1.36 g (48%). **MS(MALDI):** m/z 883.1 $[M]^+$. **Anal. Clac.** for $C_{52}H_{39}N_3S_4 \cdot CH_2Cl_2$: C, 69.26; H, 4.50; N, 4.57 %. **Found:** C, 68.99; H, 4.33; N, 5.13 %.



General procedure for synthesis of aza-BODIPY's (11-13). In a nitrogen atmosphere, the respective aza-DIPY (**8-10**) (1 eq) was dissolved in anhydrous DCM, Et_3N (5 eq) was added via syringe, followed by $BF_3 \cdot OEt_2$ (10 eq). The deep blue solution was stirred at $35^\circ C$ for 24 h and then passed through a silica plug eluted by DCM, and the pure product was obtained by precipitation with ethanol. The precipitate was collected via filtration through Celite, washed

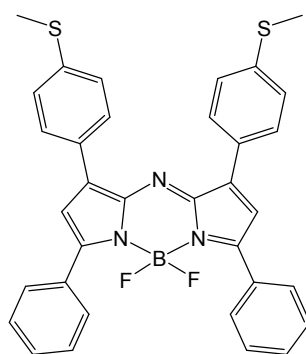
with ethanol and extracted with DCM. The solvent was removed in vacuo to yield aza-BODIPY as a dark purple solid.

8-BF₂ (11): The starting material was **8** (100 mg, 0.158 mmol), yielding a dark purple solid. Crystals were grown by the evaporation of a DCM/MeOH solution. **Yield:** 51 mg (47%). **¹H NMR** (700 MHz; CDCl₃): δ_H 7.99 (8H, dd, $J^{\beta}_{\text{HH}} = 8.4$ Hz, $J_{\text{HF}} = 4.5$ Hz, H₄+H₁₀), 7.30 (8H, d, $J^{\beta}_{\text{HH}} = 8.4$ Hz, H₃+H₁₁), 6.99 (2H, s, H₇), 2.55 (6H, s, H₁/H₃), 2.53 (6H, s, H₁/H₃) ppm. **¹³C{¹H} NMR** (176 MHz; CDCl₃): δ_C 157.9 (C₉/C₈/C₆/C₅/C₄), 145.5 (C₉/C₈/C₆/C₅/C₄), 143.1 (C₁₂/C₂), 142.8 (C₉/C₈/C₆/C₅/C₄), 140.9 (C₁₂/C₂), 129.8 (C₃/C₄), 129.4 (C₃/C₄), 129.0 (C₉/C₈/C₆/C₅/C₄), 127.7 (C₉/C₈/C₆/C₅/C₄), 125.8 (C₁₀/C₄), 125.4 (C₁₀/C₄), 117.9 (C₇), 15.3 (C₁₃/C₁), 14.8 (C₁₃/C₁) ppm. **¹⁹F NMR** (375 MHz; CDCl₃): δ_F -131.17 (dd, $J_{\text{BF}} = 63.3$ Hz, $J_{\text{FF}} = 31.6$ Hz) ppm. **MS(ASAP⁺):** *m/z* 682.145 [M+H]⁺(66%), 662.140 [M-F]⁺(100%). **Acc-MS(ASAP⁺):** *m/z* 680.1415 [M]⁺ calcd. for C₃₆H₃₀BN₃F₂S₄ *m/z* 680.1420 ($|\Delta m/z| = 0.7$ ppm). **Anal. Clac.** for C₃₆H₃₀BF₂N₃S₄·H₂O: C, 61.80; H, 4.61; N, 6.01 %. **Found:** C, 61.51; H, 4.78; N, 5.79 %.

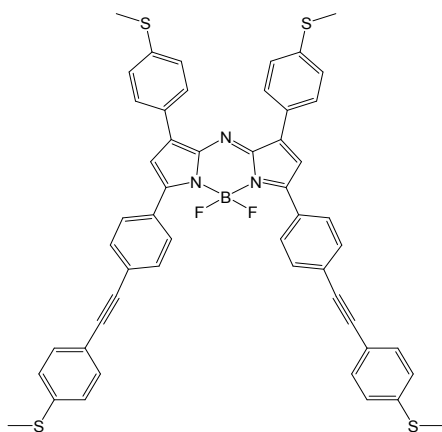


9-BF₂ (12): The starting material was **9** (300 mg, 0.55 mmol), yielding a dark purple solid. Crystals were grown by the evaporation of a DCM/MeOH solution. **Yield:** 180 mg (55%). **¹H NMR** (700 MHz; CDCl₃): δ_H 8.01 (4H, m, H₄+H₁₀), 7.47 (3H, m, H₁₁+H₁₂), 7.31 (2H, d, J^{β}_{HH}

= 8.4 Hz, H₃), 6.97 (1H, s, H₇), 2.56 (3H, s, H₁) ppm. **¹³C{¹H} NMR** (176 MHz; CDCl₃): δ_C 159.4 (C₁₃/C₈/C₆), 145.6 (C₁₃/C₈/C₆), 143.5 (C₁₃/C₈/C₆), 131.8 (C₉), 130.9 (C₁₂), 129.7 (C₁₀), 129.6 (C₄), 128.7 (C₁₁), 126.0 (C₂), 118.2 (C₇), 15.4 (C₁) ppm. **¹⁹F NMR** (375 MHz; CDCl₃): δ_F -131.10 (dd, J = 62.1, 31.1) ppm. **MS(ASAP⁺)**: *m/z* 590.174 [M+H]⁺ (100%), 570.167 [M-F]⁺ (88%). **Acc-MS(ASAP⁺)**: *m/z* 588.1652 [M]⁺ calcd. for C₃₄H₂₆BN₃F₂S₂ *m/z* 588.1666 (|Δ*m/z*| = 2.4 ppm). **Anal. Clac.** for C₃₆H₃₀BF₂N₃S₄·¼H₂O: C, 68.75; H, 4.50; N, 7.07 %. **Found**: C, 68.63; H, 4.44; N, 7.05 %.



10-BF₂ (13): The starting material was **10** (300 mg, 0.360 mmol), yielding a dark purple solid. Crystals were grown by the evaporation of a DCM/MeOH solution. **Yield**: 94 mg (30%). **¹H NMR** (700 MHz; CDCl₃): δ_H 8.06 (4H, d, *J*_{HH} = 7.8 Hz, H₁₁), 8.01 (4H, d, *J*_{HH} = 7.8 Hz, H₄), 7.61 (4H, d, *J*_{HH} = 7.7 Hz, H₁₂), 7.46 (4H, d, *J*_{HH} = 7.7 Hz, H₁₇), 7.32 (4H, d, *J*_{HH} = 7.8 Hz, H₃), 7.22 (4H, d, *J*_{HH} = 7.7 Hz, H₁₈), 7.04 (2H, s, H₇), 2.57 (6H, s, H₁), 2.51 (6H, s, H₂₀) ppm. **¹³C{¹H} NMR** (176 MHz; CDCl₃): δ_C 158.2 (C₈), 146.0 (C₉), 143.5 (C₆), 141.5 (C₂), 140.0 (C₁₉), 132.1 (C₁₇), 131.8 (C₁₂), 131.1 (C₁₀), 129.7 (C₁₁+C₄), 129.0 (C₅), 126.1 (C₁₃), 126.0 (C₃), 125.9 (C₁₈), 119.3 (C₁₆), 118.3 (C₇), 92.6 (C₁₅), 89.7 (C₁₄), 15.5 (C₁/C₂₀), 15.4 (C₁/C₂₀) ppm. **¹⁹F NMR** (375 MHz; CDCl₃): δ_F -130.90 (dd, *J*_{BF} = 65.7 Hz, *J*_{FF} = 32.8 Hz) ppm. **MS(ASAP⁺)**: *m/z* 881.210 [M+H]⁺. **Acc-MS(ASAP⁺)**: *m/z* 881.2120 [M+H]⁺ calcd. for C₅₂H₃₉BF₂N₃S₄ *m/z* 881.2124 (|Δ*m/z*| = 0.5 ppm). **Anal. Clac.** for C₅₂H₃₈BF₂N₃S₄·1¼CH₂Cl₂: C, 64.73; H, 4.13; N, 4.25 %. **Found**: C, 64.21; H, 3.79; N, 4.09 %.



2. NMR spectra of reported compounds

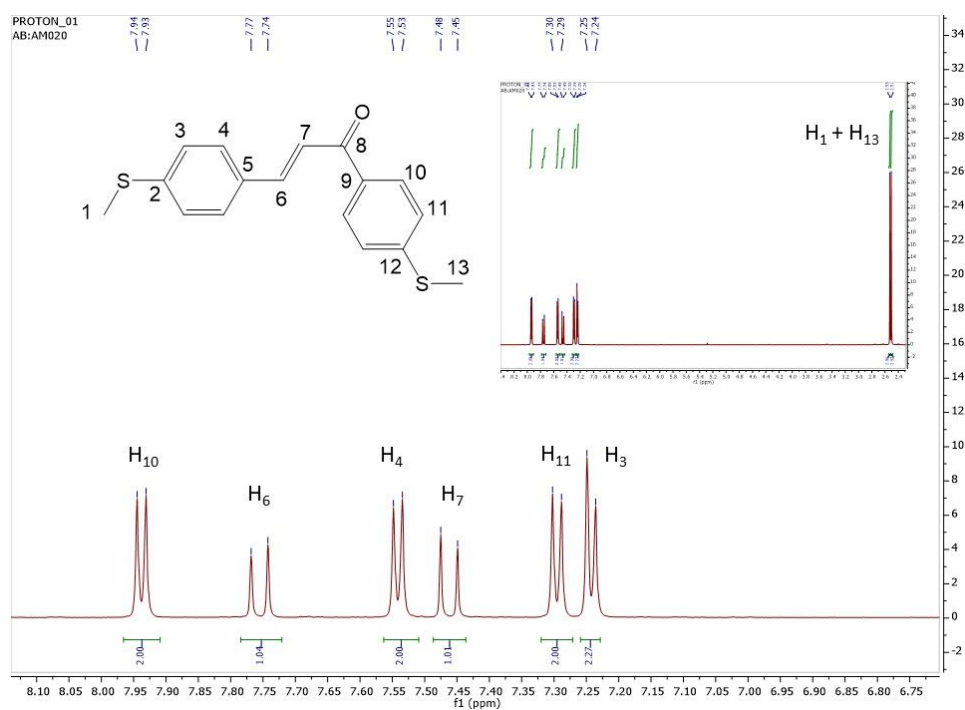


Figure S1. ¹H NMR of compound **1** recorded in CDCl₃.

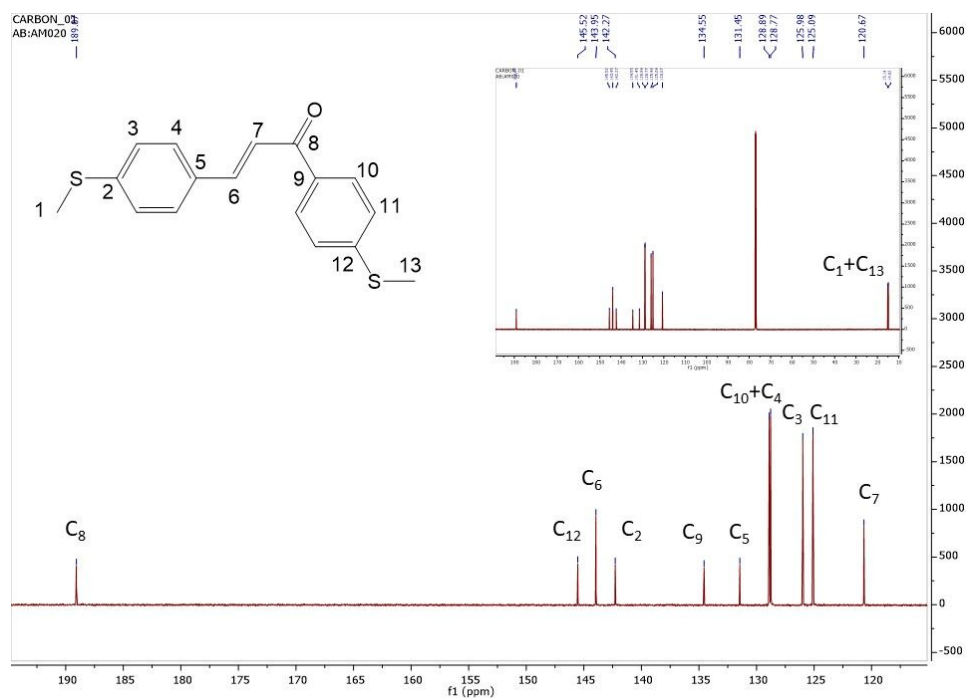


Figure S2. ¹³C NMR of compound **1** recorded in CDCl₃.

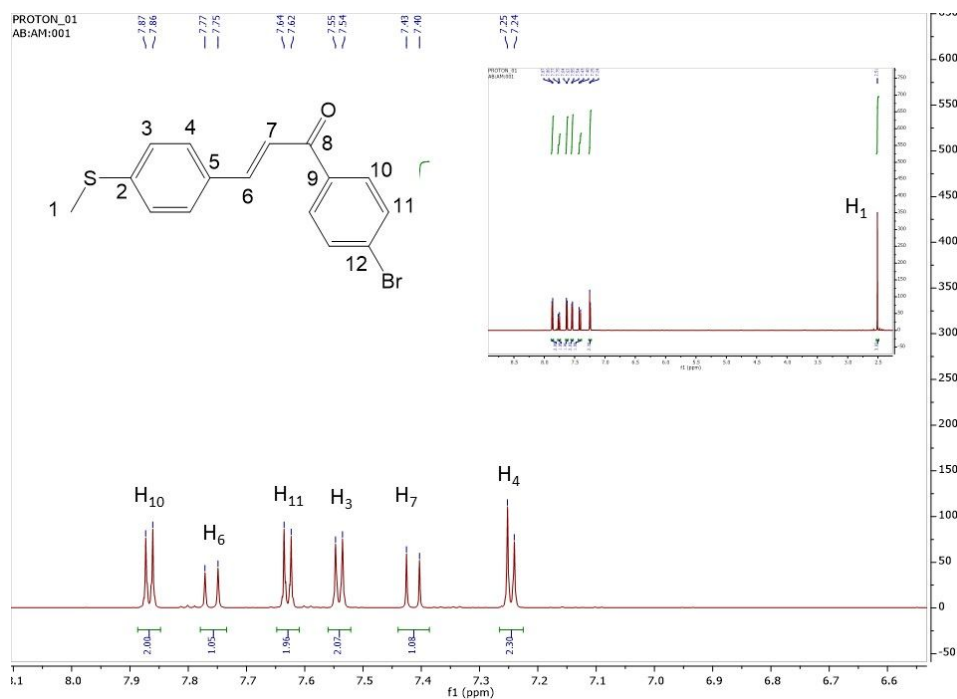


Figure S3. ¹H NMR of compound 3 recorded in CDCl₃.

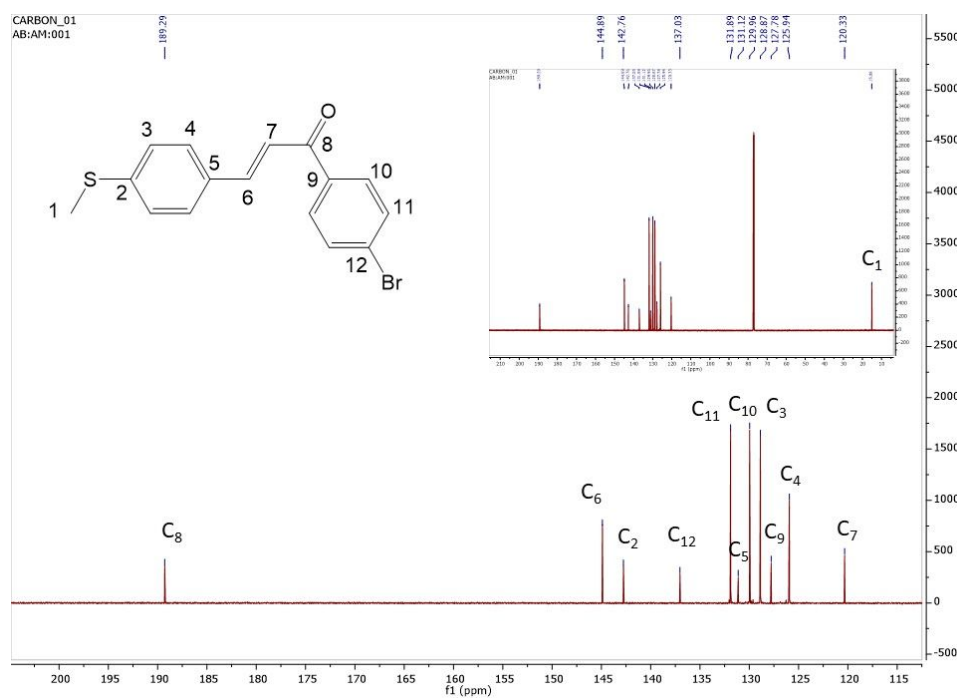


Figure S4. ¹³C NMR of compound 3 recorded in CDCl₃.

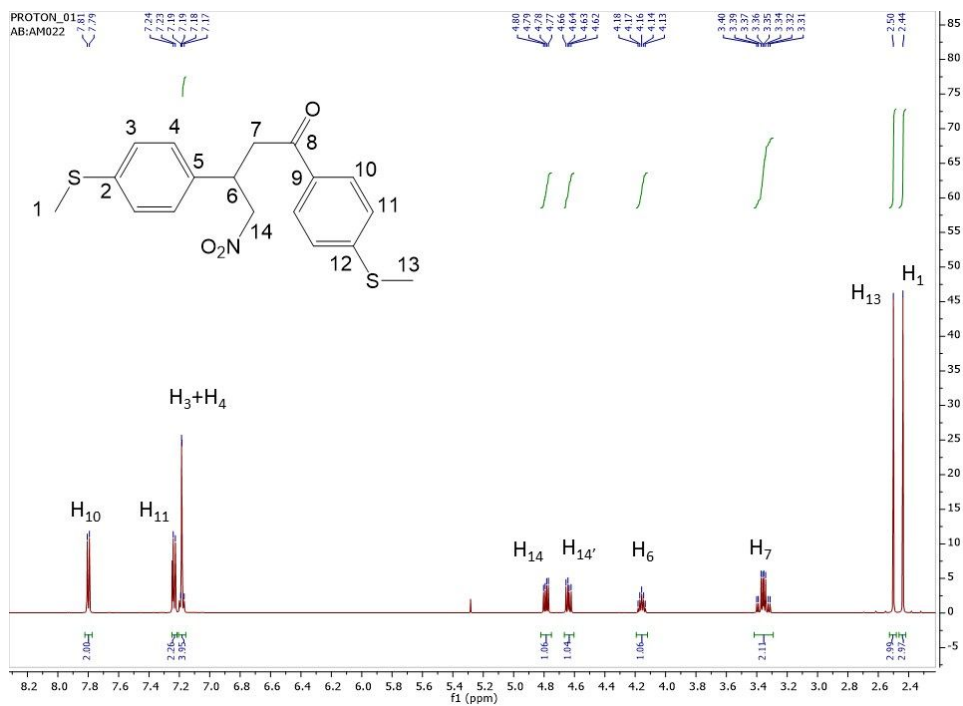


Figure S5. ¹H NMR of compound 4 recorded in CDCl₃.

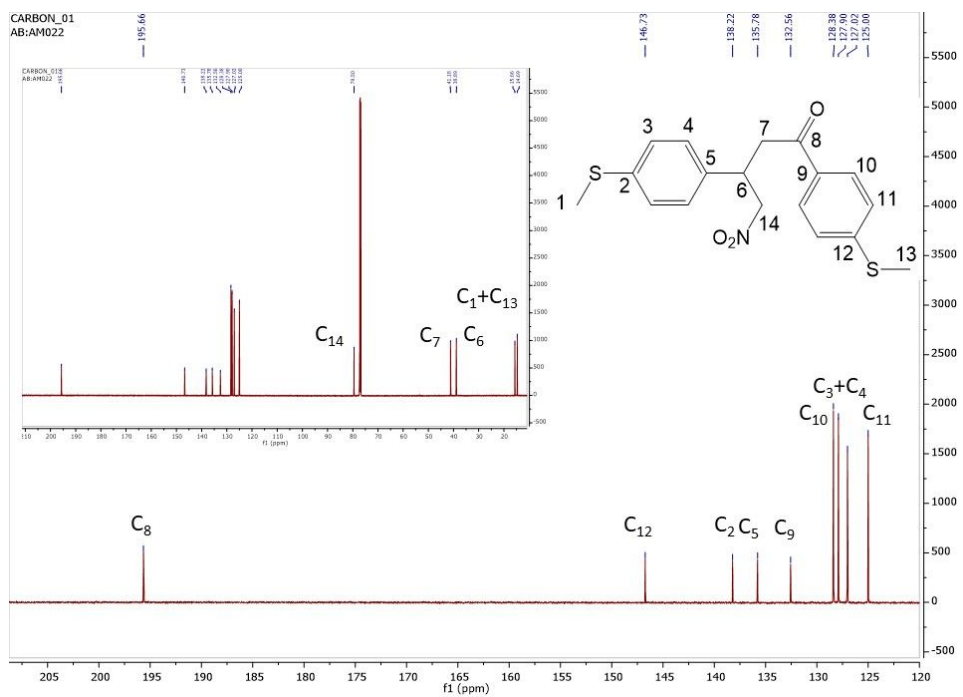


Figure S6. ¹³C NMR of compound 4 recorded in CDCl₃.

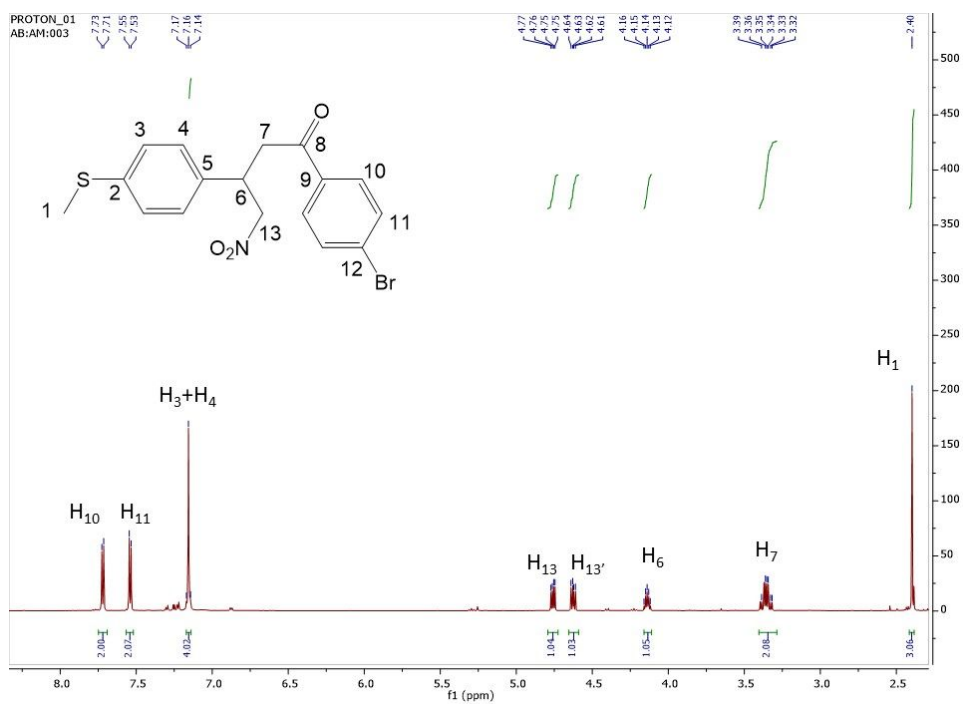


Figure S9. ¹H NMR of compound 6 recorded in CDCl₃.

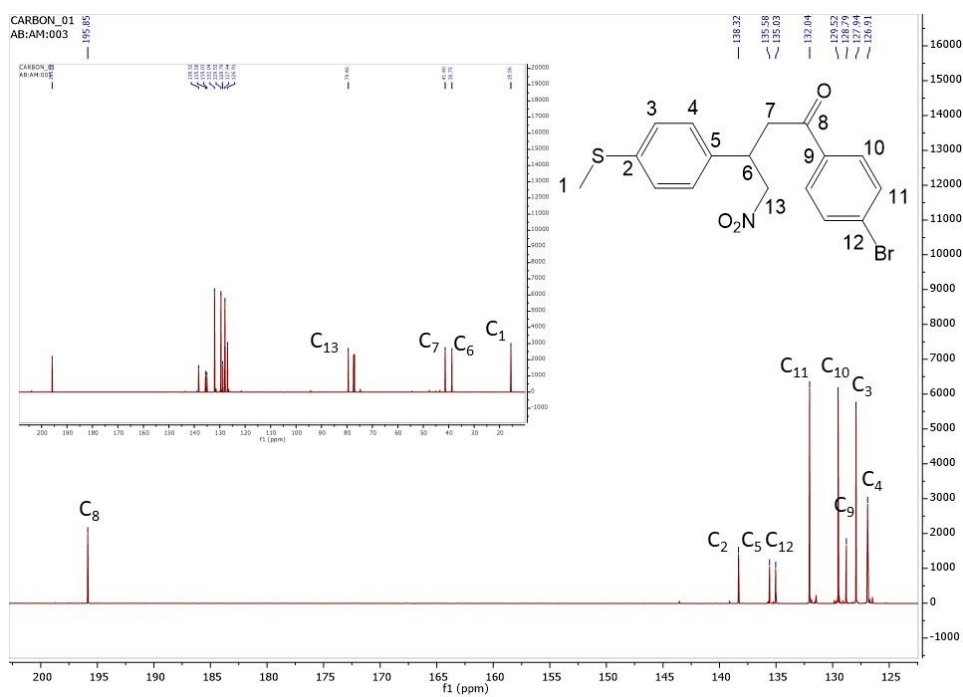


Figure S10. ¹³C NMR of compound 6 recorded in CDCl₃.

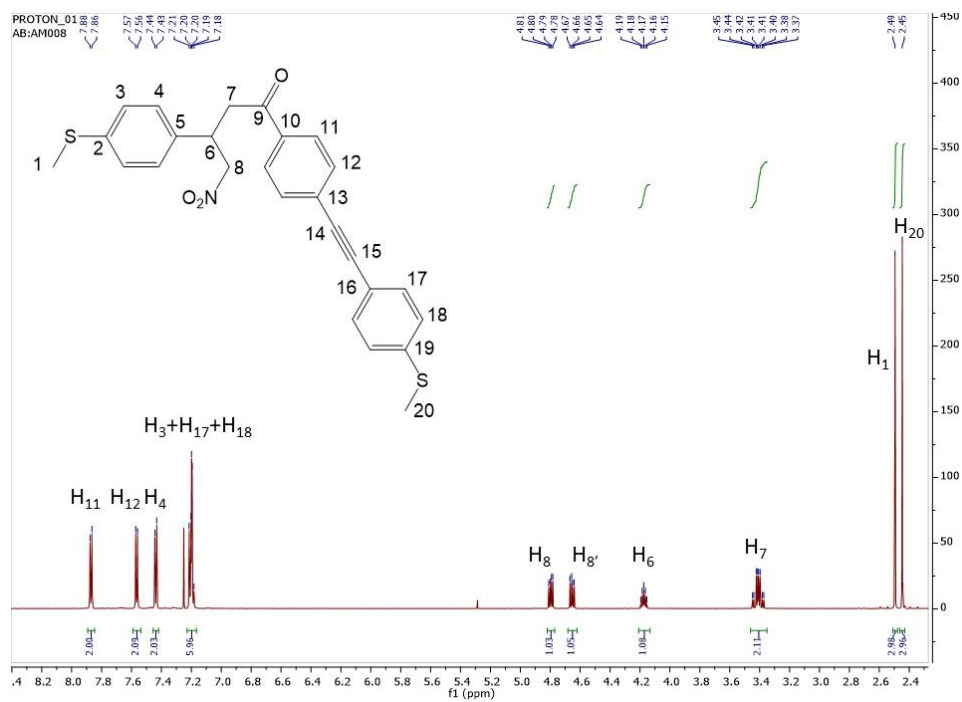


Figure S11. ¹H NMR of compound 7 recorded in CDCl₃.

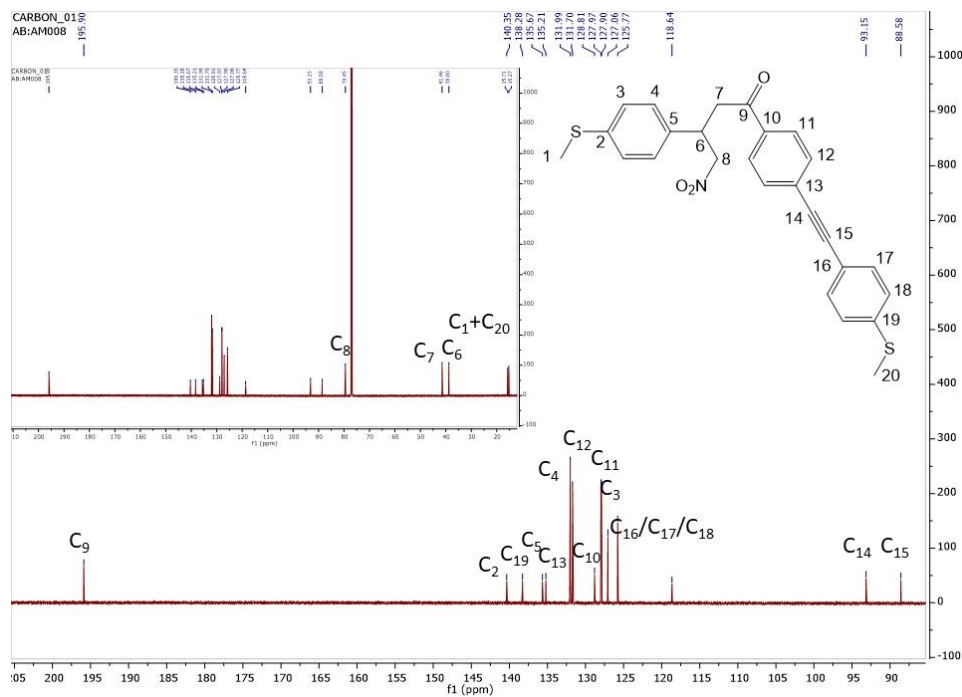


Figure S12. ¹³C NMR of compound 7 recorded in CDCl₃.

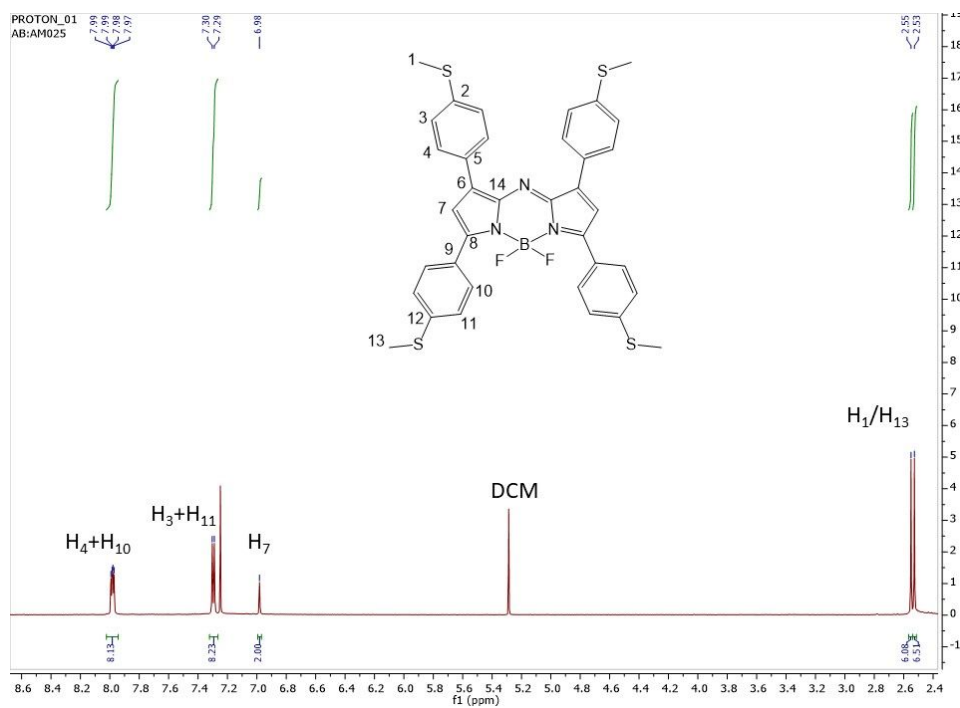


Figure S13. ¹H NMR of compound **11** recorded in CDCl₃.

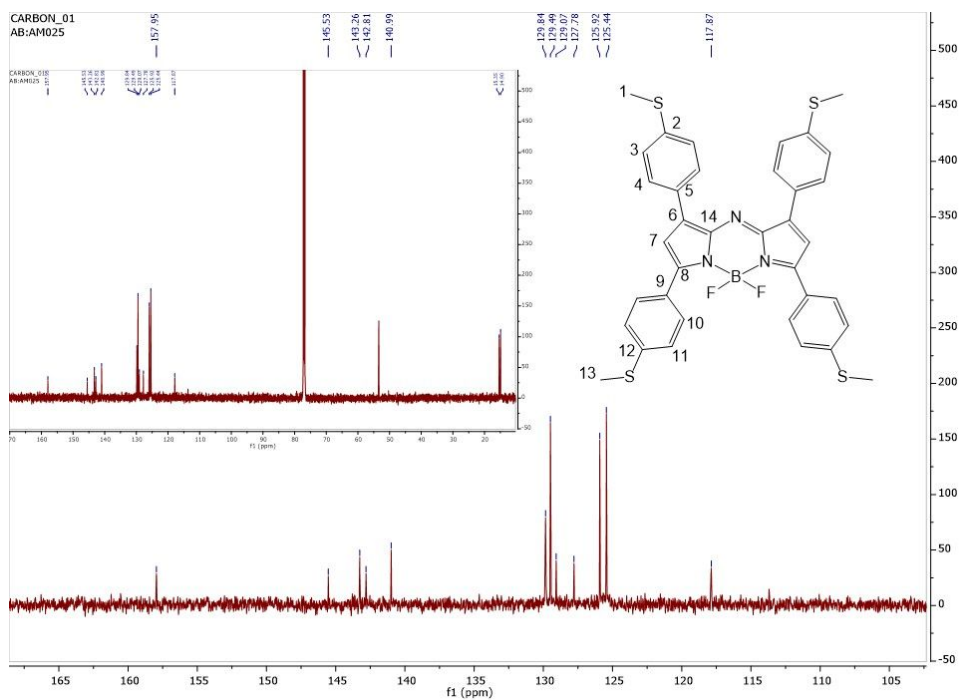


Figure S14. ¹³C NMR of compound **11** recorded in CDCl₃.

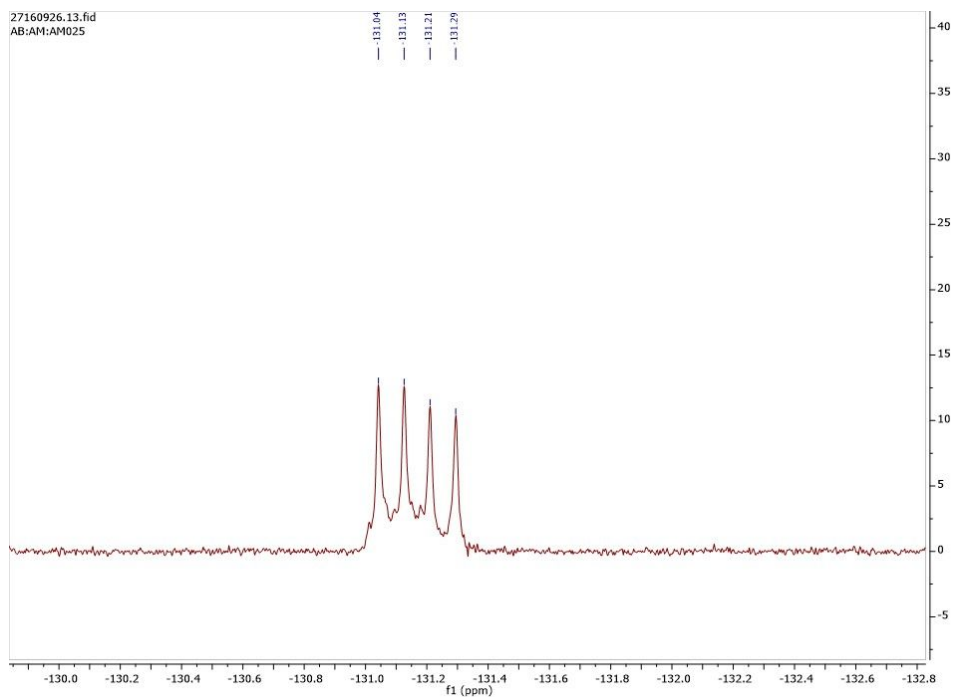


Figure S15. ^{19}F NMR of compound **11** recorded in CDCl_3 .

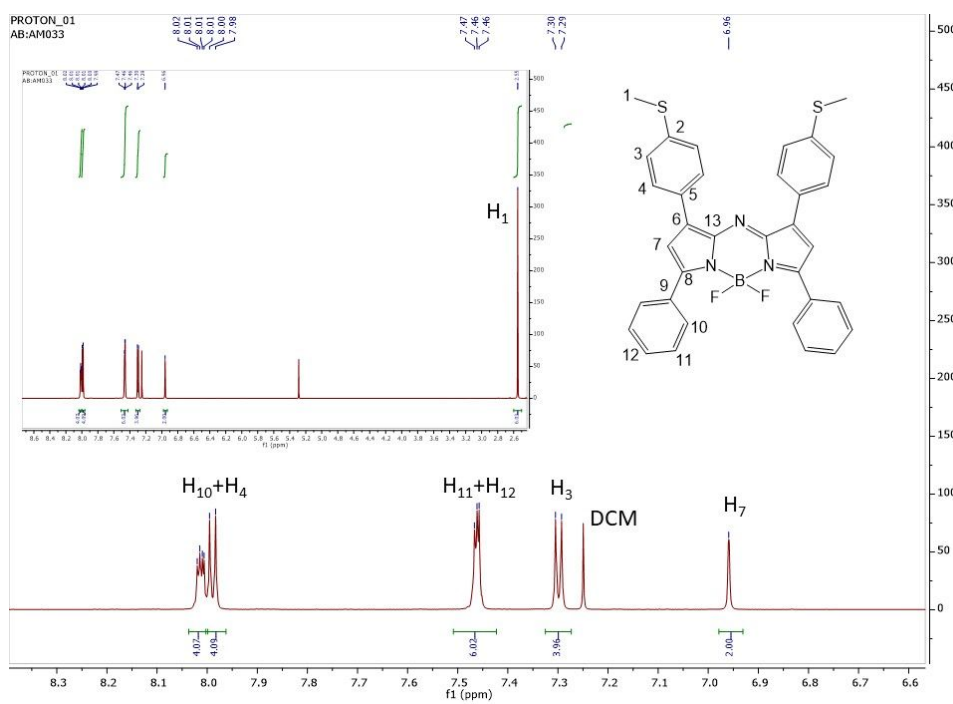


Figure S16. ^1H NMR of compound **12** recorded in CDCl_3 .

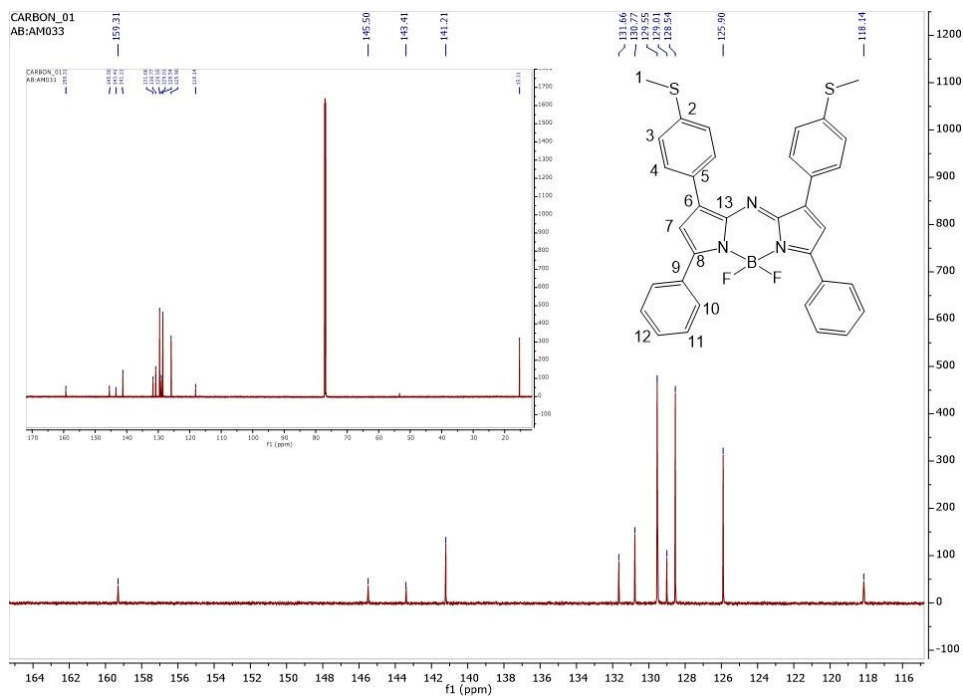


Figure S17. ^{13}C NMR of compound **12** recorded in CDCl_3 .

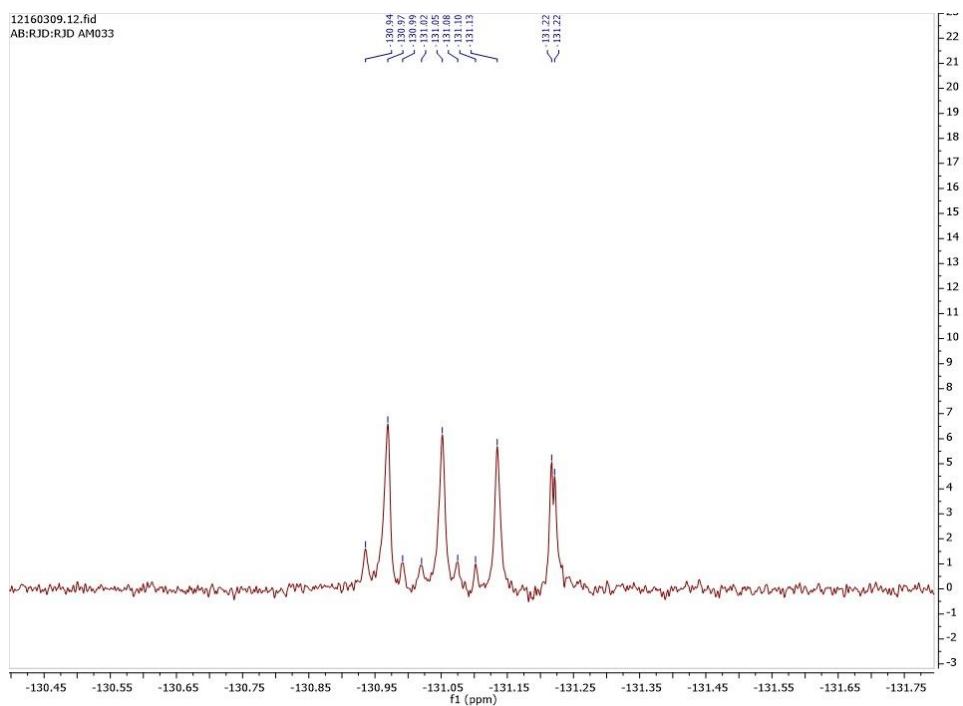


Figure S18. ^{19}F NMR of compound **12** recorded in CDCl_3 .

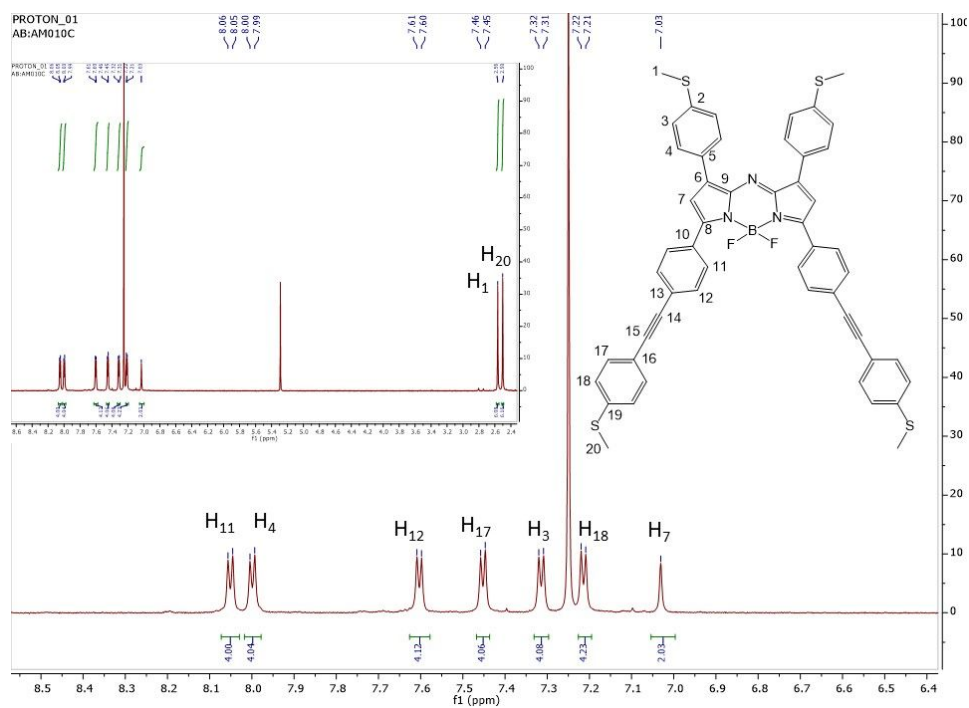


Figure S19. ¹H NMR of compound **13** recorded in CDCl₃.

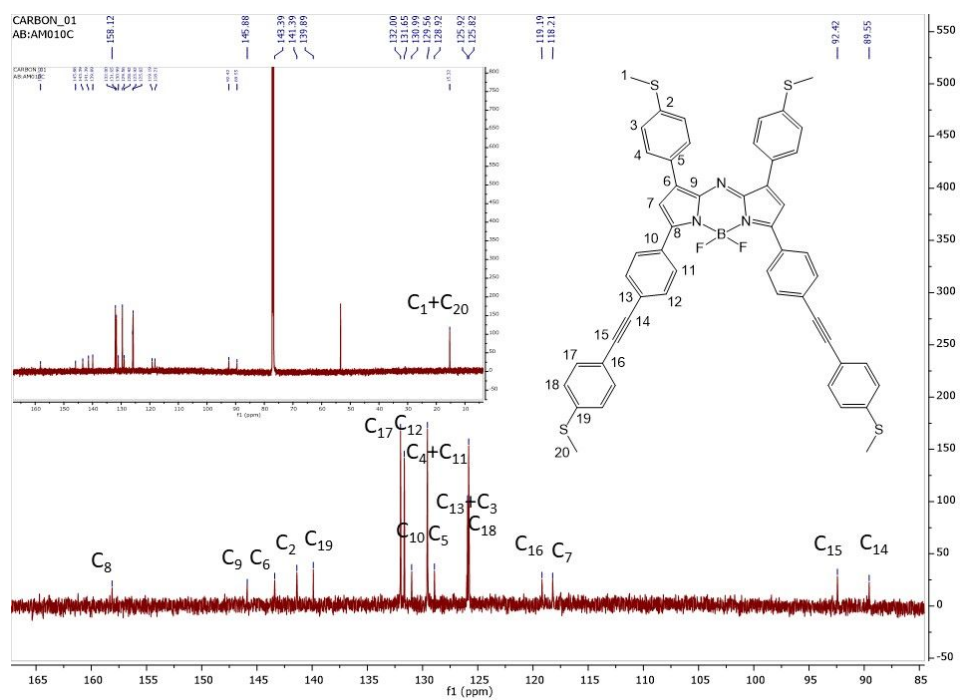


Figure S20. ¹³C NMR of compound **13** recorded in CDCl₃.

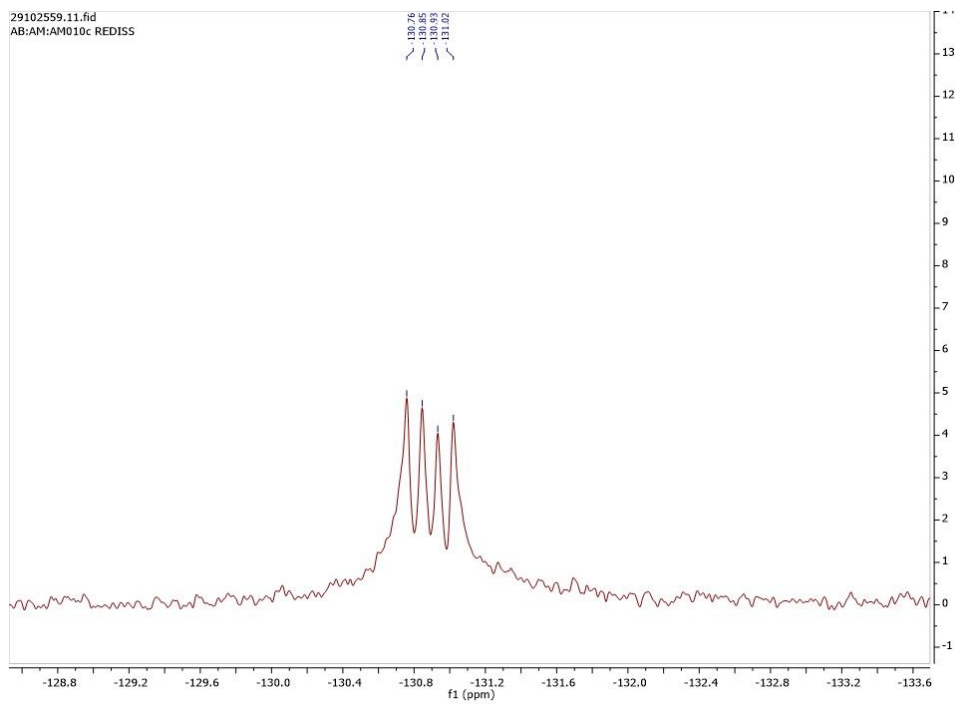


Figure S21. ^{19}F NMR of compound **13** recorded in CDCl_3 .

3. Crystallographic data

The X-ray single crystal data have been collected at the temperature 120.0(2)K using λ MoK α radiation ($\lambda = 0.71073 \text{ \AA}$) on a Bruker D8Venture (compounds **11** and **12**; Photon100 CMOS detector, I μ S-microsource, focusing mirrors) and an Agilent XCalibur (compounds **4**, **6** and **13**; Sapphire-3 CCD detector, fine-focus sealed tube, graphite monochromator) diffractometers equipped with a Cryostream (Oxford Cryosystems) open-flow nitrogen cryostats. All structures were solved by direct method and refined by full-matrix least squares on F^2 for all data using Olex2³ and SHELXTL⁴ software. All non-disordered non-hydrogen atoms were refined anisotropically, the hydrogen atoms were placed in the calculated positions and refined in riding mode. Disordered atoms in structure **12** were refined isotropically with fixed SOF=0.5. Crystal data and parameters of refinement are listed in Table S1. Crystallographic data for the structure have been deposited with the Cambridge Crystallographic Data Centre as supplementary publication CCDC 1908002-1908006.

Table S1. Crystal data and structure refinement for structures **4**, **6**, **11-13**.

Identification code	4	6	11	12	13
Empirical formula	C ₁₈ H ₁₉ NO ₃ S 2	C ₁₇ H ₁₆ BrNO ₃ S	C ₃₆ H ₃₀ BF ₂ N ₃ S 4	C ₃₄ H ₂₆ BF ₂ N ₃ S 2 x 0.5 CH ₂ Cl ₂	C ₅₂ H ₃₈ BF ₂ N ₃ S 4 x CH ₂ Cl ₂
Formula weight	361.46	394.28	681.68	631.97	966.83
Temperature/K	120.0	120.0	120.0	120.0	120.0
Crystal system	orthorhombic	orthorhombic	orthorhombic	monoclinic	triclinic
Space group	P2 ₁ 2 ₁ 2 ₁	P2 ₁ 2 ₁ 2 ₁	Pbca	P2 ₁ /c	P-1
a/Å	9.72747(17)	5.61794(14)	10.198(2)	14.9774(7)	12.2124(9)
b/Å	10.47282(17)	11.7629(2)	22.163(5)	17.4916(8)	12.8917(13)
c/Å	17.0799(4)	25.2341(4)	28.125(7)	12.2462(6)	16.7826(12)
α/°	90.00	90.00	90.00	90.00	100.946(7)
β/°	90.00	90.00	90.00	109.8080(16)	96.510(6)
γ/°	90.00	90.00	90.00	90.00	114.503(8)
Volume/Å ³	1740.00(6)	1667.56(6)	6357(3)	3018.4(2)	2305.3(3)
Z	4	4	8	4	2
ρ _{calc} , g/cm ³	1.380	1.570	1.425	1.391	1.393
μ/mm ⁻¹	0.322	2.604	0.343	0.308	0.372
F(000)	760.0	800.0	2832.0	1308.0	1000.0
Reflections collected	25351	26666	70540	62230	25376
Independent reflections, R _{int}	4637, 0.0340	4042, 0.0636	6584, 0.4179	8033, 0.0866	10579, 0.1109
Data/restraints/parameters	4637/0/219	4042/0/209	6584/0/420	8033/0/393	10579/0/590
Goodness-of-fit on F ²	1.047	1.059	0.998	1.021	0.982
Final R ₁ indexes [I ≥ 2σ (I)]	0.0305	0.0329	0.0867	0.0608	0.0768
Final wR ₂ indexes [all data]	0.0767	0.0753	0.1876	0.1536	0.1946
Largest diff. peak/hole / e Å ⁻³	0.27/-0.13	0.49/-0.32	0.36/-0.39	0.87/-1.43	0.46/-0.61
Flack parameter	-0.04(5)	-0.011(8)	n/a	n/a	n/a

Table S2. Selected bond lengths for **4**.

Atom	Atom	Length/Å	Atom	Atom	Length/Å
S1	C8	1.7635(14)	C5	C6	1.3935(19)
S1	C11	1.7948(17)	C5	C10	1.3927(18)
S2	C15	1.7621(15)	C6	C7	1.395(2)
S2	C18	1.795(2)	C7	C8	1.3886(19)
O1	N1	1.2283(18)	C8	C9	1.396(2)
O2	N1	1.2241(19)	C9	C10	1.388(2)
O3	C1	1.2201(18)	C12	C13	1.394(2)
N1	C4	1.5035(19)	C12	C17	1.398(2)
C1	C2	1.514(2)	C13	C14	1.392(2)
C1	C12	1.493(2)	C14	C15	1.393(2)
C2	C3	1.5362(19)	C15	C16	1.395(2)
C3	C4	1.532(2)	C16	C17	1.390(2)
C3	C5	1.5175(19)			

Table S3. Selected bond angles for **4**.

Atom	Atom	Atom	Angle/°	Atom	Atom	Atom	Angle/°
C8	S1	C11	103.97(7)	C8	C7	C6	120.12(13)
C15	S2	C18	103.31(8)	C7	C8	S1	124.70(12)
O1	N1	C4	118.10(13)	C7	C8	C9	118.91(13)
O2	N1	O1	123.95(15)	C9	C8	S1	116.38(10)
O2	N1	C4	117.91(14)	C10	C9	C8	120.62(13)
O3	C1	C2	121.88(13)	C9	C10	C5	120.91(13)
O3	C1	C12	121.16(13)	C13	C12	C1	122.85(13)
C12	C1	C2	116.95(12)	C13	C12	C17	118.32(13)
C1	C2	C3	113.98(12)	C17	C12	C1	118.83(13)
C4	C3	C2	105.72(11)	C14	C13	C12	121.11(14)
C5	C3	C2	113.56(11)	C13	C14	C15	120.17(15)
C5	C3	C4	112.23(11)	C14	C15	S2	123.83(12)
N1	C4	C3	111.64(12)	C14	C15	C16	119.12(14)
C6	C5	C3	121.43(12)	C16	C15	S2	117.05(12)
C10	C5	C3	120.38(12)	C17	C16	C15	120.44(14)
C10	C5	C6	118.17(13)	C16	C17	C12	120.81(14)
C5	C6	C7	121.24(13)				

Table S4. Selected bond lengths for **6**.

Atom	Atom	Length/Å		Atom	Atom	Length/Å
Br1	C7	1.901(3)		C4	C5	1.399(4)
S1	C14	1.773(3)		C4	C9	1.390(4)
S1	C17	1.790(3)		C5	C6	1.389(4)
O1	C3	1.218(3)		C6	C7	1.373(4)
O2	N1	1.219(3)		C7	C8	1.386(4)
O3	N1	1.211(3)		C8	C9	1.394(4)
N1	C10	1.502(3)		C11	C12	1.381(4)
C1	C2	1.538(4)		C11	C16	1.391(4)
C1	C10	1.527(4)		C12	C13	1.386(4)
C1	C11	1.514(4)		C13	C14	1.383(4)
C2	C3	1.513(4)		C14	C15	1.387(4)
C3	C4	1.500(4)		C15	C16	1.384(4)

Table S5. Selected bond angles for **6**.

Atom	Atom	Atom	Angle/°		Atom	Atom	Atom	Angle/°
C14	S1	C17	102.65(14)		C6	C7	Br1	119.5(2)
O2	N1	C10	118.1(2)		C6	C7	C8	122.2(2)
O3	N1	O2	123.7(3)		C8	C7	Br1	118.3(2)
O3	N1	C10	118.1(2)		C7	C8	C9	118.5(3)
C10	C1	C2	108.0(2)		C4	C9	C8	120.6(2)
C11	C1	C2	110.9(2)		N1	C10	C1	111.5(2)
C11	C1	C10	113.4(2)		C12	C11	C1	124.0(2)
C3	C2	C1	114.2(2)		C12	C11	C16	117.5(3)
O1	C3	C2	121.6(2)		C16	C11	C1	118.5(2)
O1	C3	C4	121.0(2)		C11	C12	C13	121.1(3)
C4	C3	C2	117.4(2)		C14	C13	C12	120.7(3)
C5	C4	C3	118.4(2)		C13	C14	S1	117.1(2)
C9	C4	C3	122.4(2)		C13	C14	C15	119.0(3)
C9	C4	C5	119.2(2)		C15	C14	S1	123.9(2)
C6	C5	C4	120.5(3)		C16	C15	C14	119.5(3)
C7	C6	C5	118.9(3)		C15	C16	C11	122.1(3)

Table S6. Selected bond lengths for **11**.

Atom	Atom	Length/Å		Atom	Atom	Length/Å
S1	C12	1.749(6)		C7	C8	1.419(7)
S1	C15	1.795(6)		C8	C30	1.451(7)
S2	C19	1.766(5)		C9	C10	1.403(7)
S2	C22	1.784(6)		C9	C14	1.404(7)
S3	C26	1.760(6)		C10	C11	1.378(7)
S3	C29	1.788(6)		C11	C12	1.412(7)
S4	C33	1.741(6)		C12	C13	1.376(7)
S4	C36	1.784(5)		C13	C14	1.395(7)
F1	B1	1.386(7)		C16	C17	1.386(7)
F2	B1	1.399(7)		C16	C21	1.406(7)
N1	C1	1.368(6)		C17	C18	1.378(7)
N1	C4	1.383(6)		C18	C19	1.392(7)
N1	B1	1.540(8)		C19	C20	1.373(7)
N2	C4	1.328(6)		C20	C21	1.370(7)
N2	C5	1.308(6)		C23	C24	1.391(7)
N3	C5	1.403(6)		C23	C28	1.392(7)
N3	C8	1.376(6)		C24	C25	1.393(7)
N3	B1	1.566(8)		C25	C26	1.399(8)
C1	C2	1.410(7)		C26	C27	1.375(7)
C1	C9	1.461(7)		C27	C28	1.384(7)
C2	C3	1.391(7)		C30	C31	1.402(7)
C3	C4	1.410(7)		C30	C35	1.405(7)
C3	C16	1.462(7)		C31	C32	1.360(7)
C5	C6	1.439(7)		C32	C33	1.399(8)
C6	C7	1.368(7)		C33	C34	1.397(7)
C6	C23	1.461(7)		C34	C35	1.381(7)

Table S7. Selected bond angles for **11**.

Atom	Atom	Atom	Angle/°	Atom	Atom	Atom	Angle/°
C12	S1	C15	103.0(3)	C12	C13	C14	121.1(6)
C19	S2	C22	103.7(3)	C13	C14	C9	120.9(6)
C26	S3	C29	103.2(3)	C17	C16	C3	120.9(5)
C33	S4	C36	103.8(3)	C17	C16	C21	116.4(5)
C1	N1	C4	107.1(5)	C21	C16	C3	122.8(5)
C1	N1	B1	129.6(5)	C18	C17	C16	122.4(5)
C4	N1	B1	123.0(5)	C17	C18	C19	120.0(5)
C5	N2	C4	120.4(5)	C18	C19	S2	124.1(5)
C5	N3	B1	121.0(5)	C20	C19	S2	117.3(4)
C8	N3	C5	107.2(4)	C20	C19	C18	118.6(5)
C8	N3	B1	131.3(5)	C21	C20	C19	121.3(5)
N1	C1	C2	109.1(5)	C20	C21	C16	121.4(6)
N1	C1	C9	126.5(5)	C24	C23	C6	122.0(5)
C2	C1	C9	124.3(5)	C24	C23	C28	117.6(5)
C3	C2	C1	107.9(5)	C28	C23	C6	120.4(5)
C2	C3	C4	106.0(5)	C23	C24	C25	121.1(5)
C2	C3	C16	126.3(5)	C24	C25	C26	119.7(6)
C4	C3	C16	127.6(5)	C25	C26	S3	115.9(5)
N1	C4	C3	109.8(5)	C27	C26	S3	124.3(5)
N2	C4	N1	123.7(5)	C27	C26	C25	119.7(5)
N2	C4	C3	126.3(5)	C26	C27	C28	119.8(5)
N2	C5	N3	124.6(5)	C27	C28	C23	122.0(5)
N2	C5	C6	126.6(5)	C31	C30	C8	117.5(5)
N3	C5	C6	108.6(5)	C31	C30	C35	118.6(5)
C5	C6	C23	125.5(5)	C35	C30	C8	123.9(5)
C7	C6	C5	106.3(5)	C32	C31	C30	120.7(6)
C7	C6	C23	128.2(5)	C31	C32	C33	121.7(6)
C6	C7	C8	109.1(5)	C32	C33	S4	117.6(5)
N3	C8	C7	108.7(5)	C34	C33	S4	124.8(5)
N3	C8	C30	127.6(5)	C34	C33	C32	117.7(5)
C7	C8	C30	123.7(5)	C35	C34	C33	121.5(6)
C10	C9	C1	118.4(5)	C34	C35	C30	119.9(5)
C10	C9	C14	117.6(5)	F1	B1	F2	109.6(5)
C14	C9	C1	124.0(5)	F1	B1	N1	109.5(5)
C11	C10	C9	121.1(5)	F1	B1	N3	111.3(5)
C10	C11	C12	120.9(5)	F2	B1	N1	111.3(5)
C11	C12	S1	115.7(4)	F2	B1	N3	107.8(5)
C13	C12	S1	126.0(5)	N1	B1	N3	107.2(5)
C13	C12	C11	118.3(5)				

Table S8. Selected bond lengths for **12**.

Atom	Atom	Length/Å		Atom	Atom	Length/Å
C11	C1S	1.763(8)		C8	C29	1.461(3)
C12	C1S	1.765(7)		C9	C10	1.399(3)
S1	C12	1.754(2)		C9	C14	1.398(3)
S1	C15	1.794(3)		C10	C11	1.381(3)
S2	C25	1.755(3)		C11	C12	1.392(3)
S2	C28	1.793(3)		C12	C13	1.401(3)
F1	B1	1.394(3)		C13	C14	1.376(3)
F2	B1	1.377(3)		C16	C17	1.396(4)
N1	C1	1.362(3)		C16	C21	1.396(3)
N1	C4	1.388(3)		C17	C18	1.380(4)
N1	B1	1.558(3)		C18	C19	1.378(4)
N2	C4	1.322(3)		C19	C20	1.383(4)
N2	C5	1.327(3)		C20	C21	1.382(4)
N3	C5	1.393(3)		C22	C23	1.400(3)
N3	C8	1.369(3)		C22	C27	1.393(3)
N3	B1	1.553(3)		C23	C24	1.379(4)
C1	C2	1.407(3)		C24	C25	1.394(4)
C1	C16	1.465(3)		C25	C26	1.391(4)
C2	C3	1.379(3)		C26	C27	1.384(4)
C3	C4	1.440(3)		C29	C30	1.397(3)
C3	C9	1.458(3)		C29	C34	1.391(4)
C5	C6	1.430(3)		C30	C31	1.384(4)
C6	C7	1.382(3)		C31	C32	1.375(4)
C6	C22	1.457(3)		C32	C33	1.380(4)
C7	C8	1.406(3)		C33	C34	1.388(4)

Table S9. Selected bond angles for **12**.

Atom	Atom	Atom	Angle/°	Atom	Atom	Atom	Angle/°
C11	C1S	C12	109.6(4)	C11	C12	C13	118.3(2)
C12	S1	C15	103.07(12)	C13	C12	S1	117.85(19)
C25	S2	C28	102.94(14)	C14	C13	C12	121.2(2)
C1	N1	C4	107.32(19)	C13	C14	C9	121.0(2)
C1	N1	B1	130.4(2)	C17	C16	C1	117.2(2)
C4	N1	B1	122.25(19)	C17	C16	C21	119.0(2)
C4	N2	C5	119.2(2)	C21	C16	C1	123.8(2)
C5	N3	B1	122.47(19)	C18	C17	C16	120.3(3)
C8	N3	C5	106.79(19)	C19	C18	C17	120.4(3)
C8	N3	B1	130.4(2)	C18	C19	C20	119.8(3)
N1	C1	C2	109.2(2)	C21	C20	C19	120.4(3)
N1	C1	C16	126.5(2)	C20	C21	C16	120.1(3)
C2	C1	C16	124.3(2)	C23	C22	C6	121.6(2)
C3	C2	C1	109.0(2)	C27	C22	C6	120.3(2)
C2	C3	C4	105.1(2)	C27	C22	C23	118.1(2)
C2	C3	C9	127.6(2)	C24	C23	C22	120.7(2)
C4	C3	C9	127.2(2)	C23	C24	C25	120.9(2)
N1	C4	C3	109.2(2)	C24	C25	S2	116.66(19)
N2	C4	N1	124.5(2)	C26	C25	S2	124.5(2)
N2	C4	C3	125.7(2)	C26	C25	C24	118.8(2)
N2	C5	N3	124.1(2)	C27	C26	C25	120.1(2)
N2	C5	C6	125.3(2)	C26	C27	C22	121.4(2)
N3	C5	C6	109.6(2)	C30	C29	C8	118.5(2)
C5	C6	C22	125.1(2)	C34	C29	C8	122.7(2)
C7	C6	C5	105.4(2)	C34	C29	C30	118.7(2)
C7	C6	C22	129.3(2)	C31	C30	C29	120.0(3)
C6	C7	C8	108.9(2)	C32	C31	C30	121.0(3)
N3	C8	C7	109.3(2)	C31	C32	C33	119.5(2)
N3	C8	C29	125.3(2)	C32	C33	C34	120.3(3)
C7	C8	C29	125.4(2)	C33	C34	C29	120.5(2)
C10	C9	C3	119.5(2)	F1	B1	N1	109.26(19)
C14	C9	C3	123.1(2)	F1	B1	N3	109.9(2)
C14	C9	C10	117.4(2)	F2	B1	F1	110.8(2)
C11	C10	C9	122.0(2)	F2	B1	N1	110.8(2)
C10	C11	C12	120.1(2)	F2	B1	N3	110.31(19)
C11	C12	S1	123.82(19)	N3	B1	N1	105.63(19)

Table S10. Selected bond lengths for **13**.

Atom	Atom	Length/Å		Atom	Atom	Length/Å
C11	C1S	1.770(6)		C13	C14	1.374(6)
C12	C1S	1.745(6)		C15	C16	1.190(6)
S1	C20	1.757(5)		C16	C17	1.444(6)
S1	C23	1.783(5)		C17	C18	1.387(7)
S2	C27	1.764(5)		C17	C22	1.396(6)
S2	C30	1.790(6)		C18	C19	1.377(6)
S3	C49	1.760(4)		C19	C20	1.396(6)
S3	C52	1.797(5)		C20	C21	1.389(7)
S4	C42	1.762(5)		C21	C22	1.386(6)
S4	C45	1.779(5)		C24	C25	1.397(6)
F1	B1	1.393(6)		C24	C29	1.403(6)
F2	B1	1.369(7)		C25	C26	1.382(6)
N1	C1	1.371(6)		C26	C27	1.388(7)
N1	C4	1.399(5)		C27	C28	1.403(7)
N1	B1	1.577(6)		C28	C29	1.390(6)
N2	C4	1.315(6)		C31	C32	1.396(6)
N2	C5	1.331(5)		C31	C36	1.395(5)
N3	C5	1.396(5)		C32	C33	1.387(6)
N3	C8	1.379(5)		C33	C34	1.403(6)
N3	B1	1.557(6)		C34	C35	1.403(6)
C1	C2	1.404(6)		C34	C37	1.466(6)
C1	C9	1.459(6)		C35	C36	1.380(6)
C2	C3	1.383(6)		C37	C38	1.160(6)
C3	C4	1.445(6)		C38	C39	1.453(6)
C3	C24	1.461(6)		C39	C40	1.389(7)
C5	C6	1.426(6)		C39	C44	1.388(6)
C6	C7	1.367(6)		C40	C41	1.376(6)
C6	C46	1.473(6)		C41	C42	1.391(7)
C7	C8	1.415(6)		C42	C43	1.375(7)
C8	C31	1.463(6)		C43	C44	1.387(6)
C9	C10	1.413(6)		C46	C47	1.398(6)
C9	C14	1.394(6)		C46	C51	1.397(6)
C10	C11	1.377(6)		C47	C48	1.381(6)
C11	C12	1.414(6)		C48	C49	1.404(6)
C12	C13	1.381(7)		C49	C50	1.392(6)
C12	C15	1.431(6)		C50	C51	1.384(6)

Table S11. Selected bond angles for **13**.

Atom	Atom	Atom	Angle/°	Atom	Atom	Atom	Angle/°
C12	C1S	C11	111.2(3)	C21	C20	C19	118.8(5)
C20	S1	C23	104.0(2)	C22	C21	C20	120.6(5)
C27	S2	C30	103.7(3)	C21	C22	C17	120.4(5)
C49	S3	C52	103.1(2)	C25	C24	C3	120.0(4)
C42	S4	C45	103.3(3)	C25	C24	C29	117.2(4)
C1	N1	C4	107.1(4)	C29	C24	C3	122.8(4)
C1	N1	B1	130.5(4)	C26	C25	C24	122.3(5)
C4	N1	B1	122.3(4)	C25	C26	C27	120.0(4)
C4	N2	C5	119.8(4)	C26	C27	S2	125.0(4)
C5	N3	B1	122.5(4)	C26	C27	C28	119.1(4)
C8	N3	C5	105.9(4)	C28	C27	S2	116.0(4)
C8	N3	B1	131.4(4)	C29	C28	C27	120.2(5)
N1	C1	C2	109.0(4)	C28	C29	C24	121.2(4)
N1	C1	C9	125.6(4)	C32	C31	C8	117.7(4)
C2	C1	C9	125.4(4)	C36	C31	C8	124.1(4)
C3	C2	C1	109.8(4)	C36	C31	C32	118.2(4)
C2	C3	C4	104.7(4)	C33	C32	C31	121.5(4)
C2	C3	C24	128.4(4)	C32	C33	C34	119.8(4)
C4	C3	C24	126.8(4)	C33	C34	C37	121.6(4)
N1	C4	C3	109.3(4)	C35	C34	C33	118.8(4)
N2	C4	N1	124.0(4)	C35	C34	C37	119.6(4)
N2	C4	C3	126.4(4)	C36	C35	C34	120.5(4)
N2	C5	N3	124.0(4)	C35	C36	C31	121.2(4)
N2	C5	C6	125.4(4)	C38	C37	C34	175.2(5)
N3	C5	C6	109.7(4)	C37	C38	C39	174.6(5)
C5	C6	C46	124.7(4)	C40	C39	C38	121.1(5)
C7	C6	C5	106.3(4)	C44	C39	C38	121.0(5)
C7	C6	C46	128.9(4)	C44	C39	C40	117.8(4)
C6	C7	C8	108.4(4)	C41	C40	C39	121.4(5)
N3	C8	C7	109.6(4)	C40	C41	C42	120.6(5)
N3	C8	C31	125.3(4)	C41	C42	S4	116.5(4)
C7	C8	C31	125.1(4)	C43	C42	S4	125.2(4)
C10	C9	C1	117.8(4)	C43	C42	C41	118.3(4)
C14	C9	C1	123.9(5)	C42	C43	C44	121.3(5)
C14	C9	C10	118.2(4)	C43	C44	C39	120.6(5)
C11	C10	C9	120.5(4)	C47	C46	C6	122.2(4)
C10	C11	C12	120.9(5)	C51	C46	C6	119.3(4)
C11	C12	C15	121.8(5)	C51	C46	C47	118.5(4)
C13	C12	C11	117.6(4)	C48	C47	C46	120.9(4)
C13	C12	C15	120.6(4)	C47	C48	C49	120.5(4)
C14	C13	C12	122.2(4)	C48	C49	S3	116.2(4)
C13	C14	C9	120.6(5)	C50	C49	S3	125.1(4)
C16	C15	C12	176.3(5)	C50	C49	C48	118.7(4)
C15	C16	C17	179.4(5)	C51	C50	C49	120.7(4)
C18	C17	C16	120.6(4)	C50	C51	C46	120.8(4)

Table S11 continued. Selected bond angles for **13**.

Atom	Atom	Atom	Angle/°		Atom	Atom	Atom	Angle/°
C18	C17	C22	118.6(5)		F1	B1	N1	109.5(4)
C22	C17	C16	120.8(5)		F1	B1	N3	108.8(4)
C19	C18	C17	121.2(5)		F2	B1	F1	111.7(4)
C18	C19	C20	120.4(5)		F2	B1	N1	110.3(4)
C19	C20	S1	116.1(4)		F2	B1	N3	111.4(4)
C21	C20	S1	125.1(4)		N3	B1	N1	104.9(3)

b) Photophysical Measurements

UV-Visible spectra were obtained using quartz cells of 1 cm path length on a Unicam UV2-100 spectrometer, and processed using Unicam Vision software. Emission spectra were recorded on a Horiba Jobin Yvon SPEX Fluorolog 3-22 spectrofluorometer, and processed using Fluorolog 3-22 and DataMax software. Fluorescence lifetimes were determined using a custom spectrometer; measured by time-correlated single photon counting using a pulsed diode laser (371 or 396 nm), made by IBH Ltd, running at 1 MHz. The fluorescence emission was collected at right angles to the excitation source, the emission wavelength was selected using a Horiba Jobin Yvon Triax 190 monochromator and detected by a cooled IBH TBX-04 PMT. Timing was achieved using an Ortec 567 time-to-amplitude converter and an E. G. & G Trumpcard pulse height analyzer (PHA), and data was recorded using Maestro (ver. 5.10) software. Photoluminescence quantum yield measurements were carried out using the relative method⁵ with LDS751 in methanol as the standard and 4 solutions at different concentrations for each sample. Absorbance measurements were recorded using a Unicam UV2-100 spectrometer with 2 cm path length quartz cells, followed by correction for absorbance of solvent as well as baseline shifts. Fluorescence measurements were recorded using a custom system; samples were measured in 1 cm path length quartz fluorescence cuvettes. A temperature stabilized 532 nm laser diode was used for excitation, emission was recorded at right angles using an Ocean Optics Maya 2000 pro CCD spectrometer. Spectra were recorded using Ocean Optics Spectra Suite software and corrected using MATLAB software for dark current, sensitivity, refractive index of the solvent and power of the excitation source which was measured using a Thor Labs PDA36A photodiode.

1. PLQY measurement

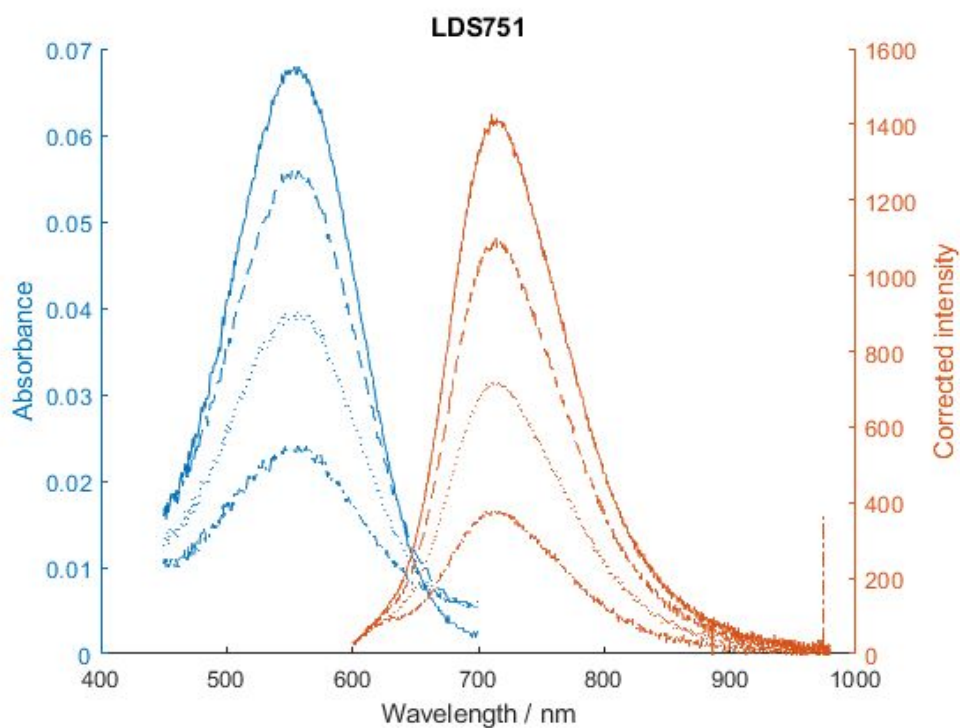


Figure S22. Absorbance and emission spectra of the standard (LDS751 in MeOH) used for PLQY calculations.

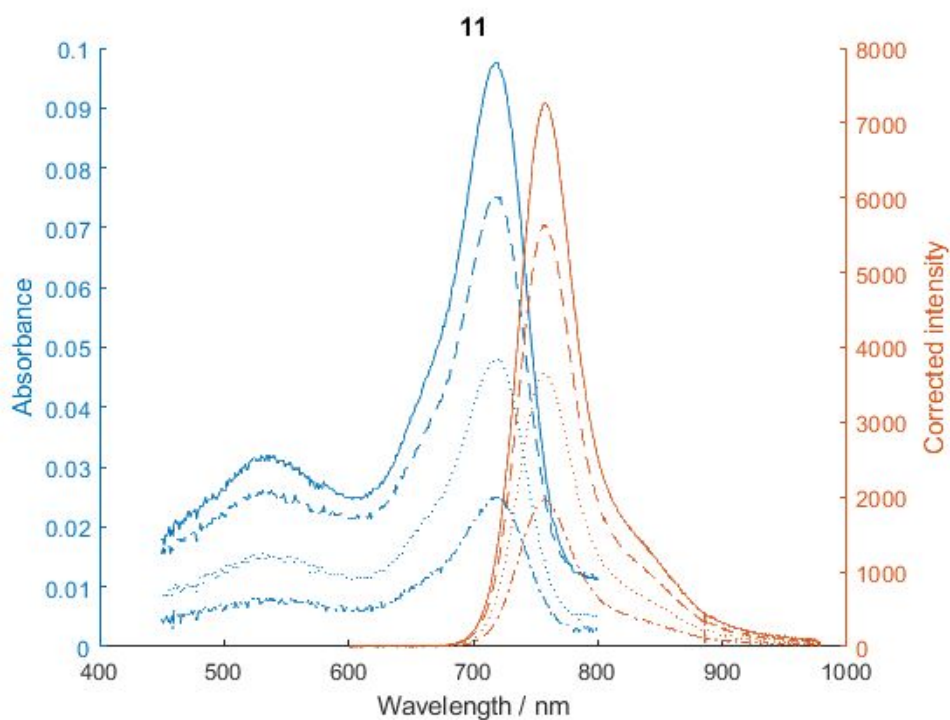


Figure S23. Absorbance and emission spectra of **11** used for PLQY calculations.

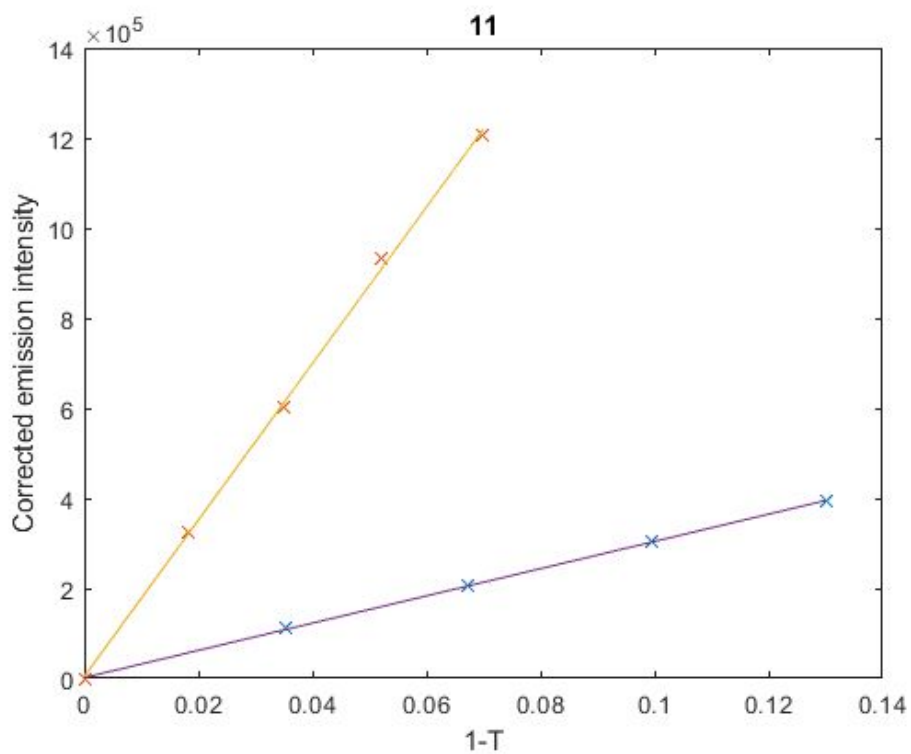


Figure S24. Correlated emission intensity and 1-T(532 nm) for **11** (yellow) and LDS752 (purple).

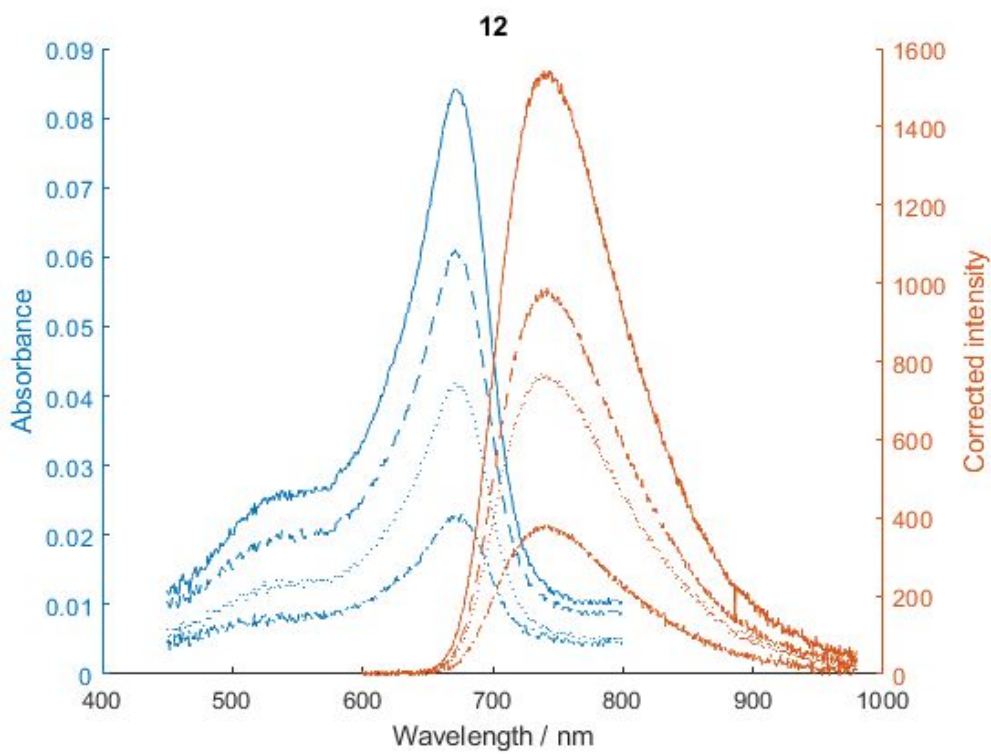


Figure S25. Absorbance and emission spectra of **12** used for PLQY calculations.

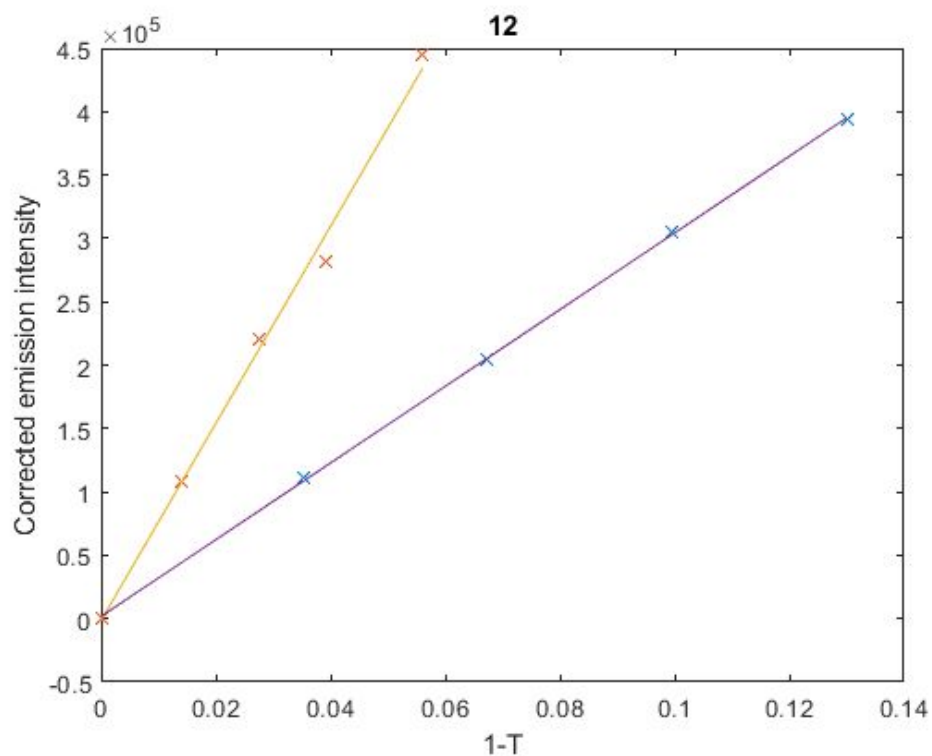


Figure S26. Correlated emission intensity and 1-T(532 nm) for **12** (yellow) and LDS751 (purple).

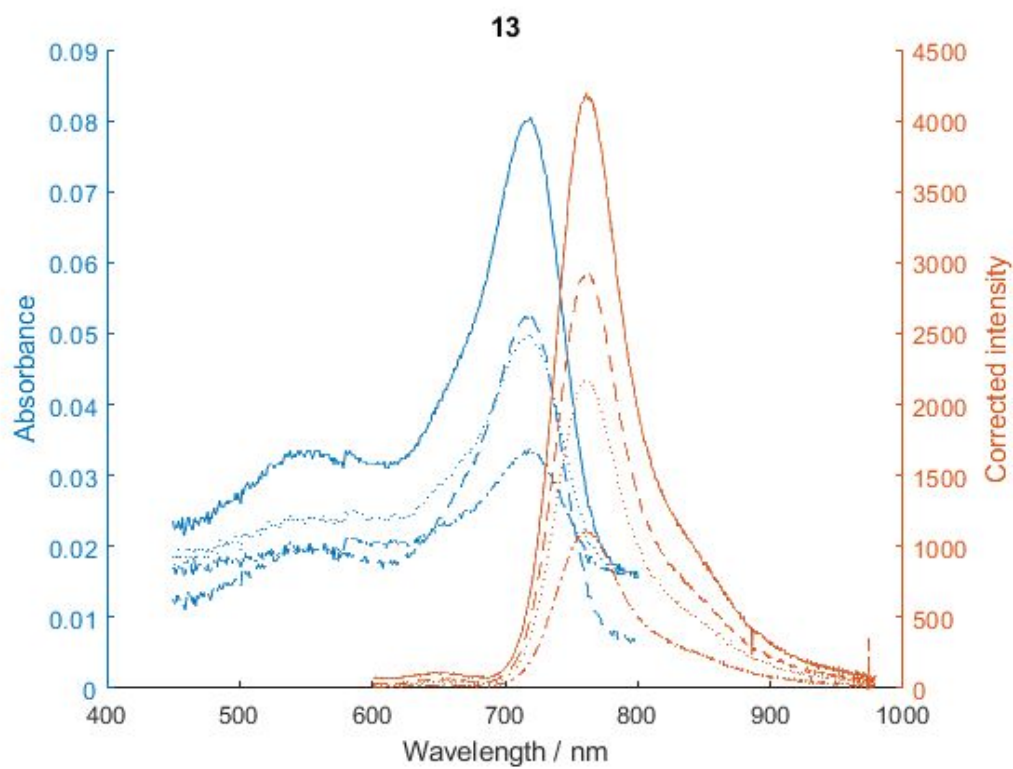


Figure S27. Absorbance and emission spectra of **13** used for PLQY calculations.

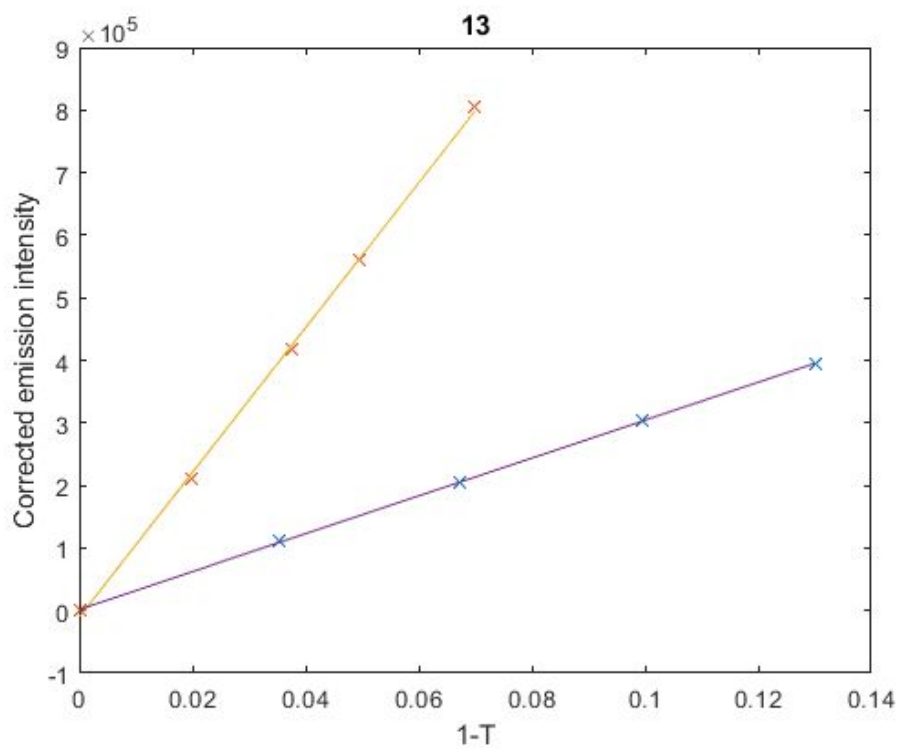


Figure S28. Correlated emission intensity and $1-T(532\text{ nm})$ for **13** (yellow) and LDS751 (purple).

2. Solvatochromism

Table S12. Photochemical data for aza-BODPYs **11-13**.

Compound	Solvent	Absorption, nm ($\epsilon \times 10^3$, L mol ⁻¹ cm ⁻¹)	S ₁ -S ₀ , eV	Emission, nm	Lifetime, ns	PLQY
Aza-BOPY ⁶		468 (6.0), 647 (85)		682	0.78	0.30
11	DCM	717 (93), 536 (25), 367 (sh,19), 326 (28), 272 (55)	1.618	758	2.6	0.71
	THF	720				
	EtOAc	715				
	CHCl ₃	718				
12	DCM	672 (92), 535 (sh, 21), 312 (43), 270 (41)	1.717	735	1.7	0.32
	THF	675				
	EtOAc	669				
	CHCl ₃	673				
	Toluene	677				
13	DCM	717 (79), 552 (23), 379 (sh, 25), 331 (59), 288 (42)	1.633	761	2.0	0.47
	THF	719				
	EtOAc	718				
	CHCl ₃	718				
	Toluene	713				

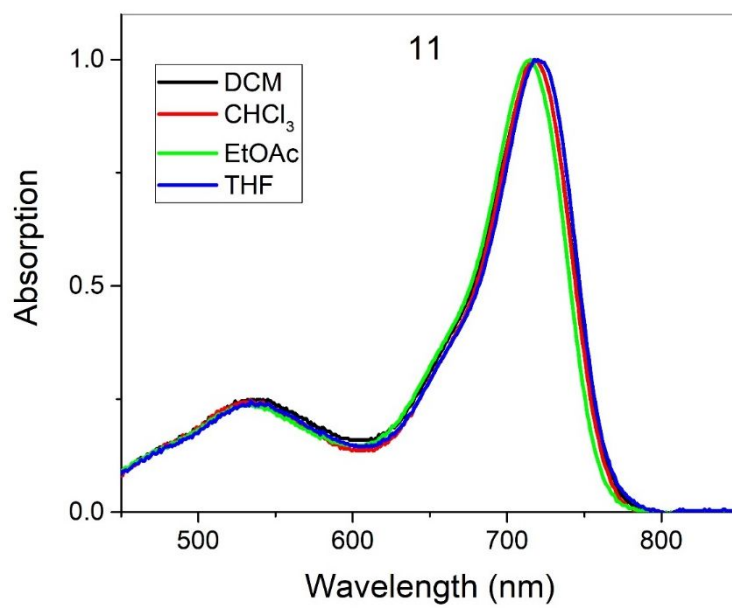


Figure S29. Electronic absorption spectra of **11**.

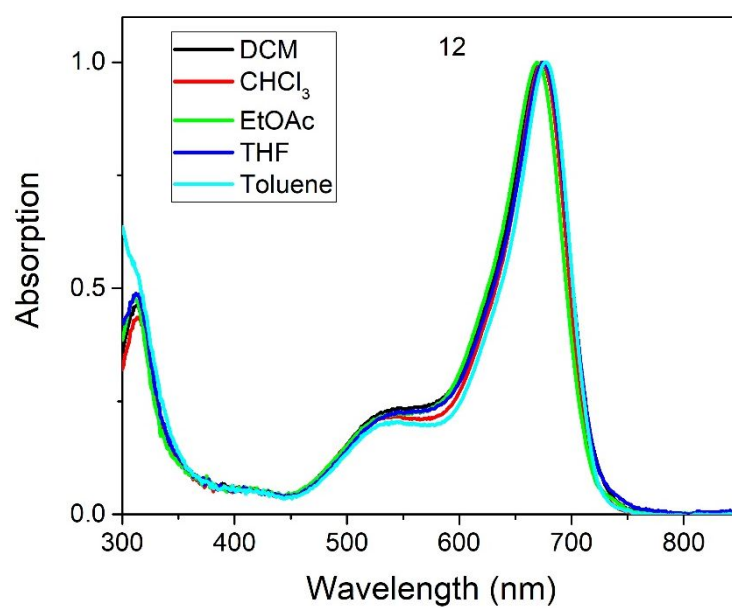


Figure S30. Electronic absorption spectra of **12**.

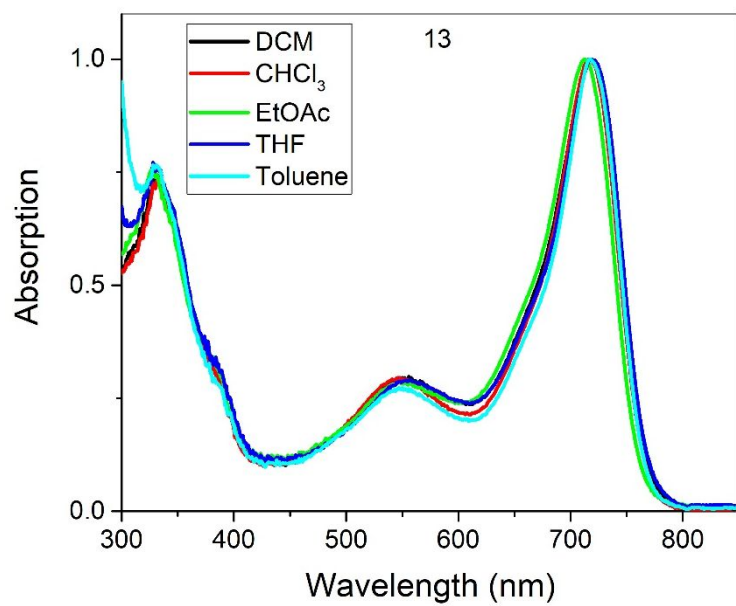


Figure S31. Electronic absorption spectra of **13**.

3. Computational

Density functional theory (DFT) calculations were carried out using the Gaussian 09 package (Gaussian, Inc)⁷, all results were displayed using GaussView⁸ and GaussSum⁹. All calculations used the B3LYP level set employing a 6-31G(d)/LANL2DZ basis set, geometrically optimized in a DCM solvent field using the SCRF-PCM method, with energy minima confirmed by frequency calculations.

Table S13. First 10 excitations of **11**.

Energy (cm ⁻¹)	Wavelength (nm)	Osc. Strength	Symmetry	Major contributions
14389.73	694.93	0.890	Singlet-B	HOMO→LUMO (98%)
16931.99	590.59	0.046	Singlet-B	H-1→LUMO (96%)
17196.54	581.51	0.689	Singlet-A	H-2→LUMO (99%)
20651.82	484.21	0.121	Singlet-A	H-3→LUMO (98%)
23575.58	424.16	0.038	Singlet-B	H-4→LUMO (89%)
26047.67	383.91	0.005	Singlet-B	H-7→LUMO (10%), H-5→LUMO (82%)
26342.87	379.60	0.002	Singlet-A	H-6→LUMO (99%)
26832.45	372.68	0.008	Singlet-B	H-7→LUMO (86%)
27176.04	367.90	0.002	Singlet-A	H-8→LUMO (98%)
27405.10	364.89	0.015	Singlet-B	H-9→LUMO (97%)

Table S14. First 10 excitations of **12**.

Energy (cm ⁻¹)	Wavelength (nm)	Osc. Strength	Symmetry	Major contributions
14825.27	674.52	0.592	Singlet-B	HOMO→LUMO (92%)
17239.29	580.07	0.479	Singlet-A	H-1→LUMO (99%)
18398.31	543.52	0.288	Singlet-B	H-2→LUMO (89%)
25528.25	391.72	0.001	Singlet-B	H-6→LUMO (69%), H-4→LUMO (25%)
25791.99	387.71	0.008	Singlet-A	H-3→LUMO (86%)
25866.20	386.60	0.008	Singlet-B	H-6→LUMO (24%), H-4→LUMO (73%)
26018.63	384.33	0.001	Singlet-A	H-7→LUMO (91%)
26325.93	379.85	0.006	Singlet-B	H-8→LUMO (93%)
26770.34	373.54	0.172	Singlet-A	H-9→LUMO (36%), H-5→LUMO (58%)
27069.57	369.41	0.040	Singlet-A	H-9→LUMO (62%), H-5→LUMO (31%)

Table S15. First 10 excitations of **13**.

Energy (cm ⁻¹)	Wavelength (nm)	Osc. Strength	Symmetry	Major contributions
13347.66	749.19	1.055	Singlet-B	HOMO→LUMO (100%)
15631.02	639.75	0.000	Singlet-B	H-2→LUMO (96%)
15747.16	635.03	1.048	Singlet-A	H-1→LUMO (91%)
17607.08	567.95	0.025	Singlet-A	H-3→LUMO (90%)
19732.35	506.78	0.127	Singlet-B	H-4→LUMO (92%)
24757.18	403.92	0.001	Singlet-A	H-5→LUMO (87%), HOMO→L+1 (10%)
25232.24	396.31	0.003	Singlet-B	H-7→LUMO (86%), H-6→LUMO (10%)
25674.24	389.49	0.001	Singlet-A	H-8→LUMO (99%)
25884.75	386.32	0.001	Singlet-B	H-9→LUMO (63%), H-6→LUMO (32%)
26308.19	380.10	1.714	Singlet-A	HOMO→L+1 (82%)

c) Conductance measurements

Single molecular conductance measurements were performed with a bespoke break junction scanner and an Agilent Picoscan 5500 STM-AFM equipment using Picoscan 5.3.3 software. Arrandee gold on glass slides Au (111) were used to perform the electrical measurements and the gold slides were flame annealed prior to measurements, generating Au (111) flat terraces.¹⁰ Sample solutions (10^{-4} M) were prepared in a tetrahydrofuran:mesitylene solution (THF:Mes, 1:4) and 100 μ L of the solution was placed into the liquid STM cell for the measurements. Gold tips were freshly mechanically etched from 0.25 mm gold wire (99.99%) for each experiment. The STM-BJ tip was repeatedly brought into contact with the surface and a set point of 100 μ A was applied to achieve the contact formation between tip and sample. Once the contact was formed, the tip was withdrawn 4 nm with a withdrawal rate of 20 nm s⁻¹. The bias voltage was -100 mV applied between the tip and substrate. The process was repeated ~4000 times for each sample, after which the current versus distance traces were compiled into histograms. The peaks obtained in the histogram determine the most likely conductance for a single molecule junction. An automated program was used to create the histograms from the raw data, which also rejects some curves with excessive noise or extremely long decay times.

Conductance measurements for the molecules **11**, **12** and **13** were performed in various solvents and deposition methods. Samples measured in air conditions were prepared by immersing a fresh annealed gold slide into a 1 mM molecule solution in chloroform during 10 minutes, allowing that way to the molecules to deposit on the flat gold surface. Samples were then rinsed with ethanol after extracting them from the solution and dried with nitrogen gas flow. Samples measured in solution were prepared by adding 100 μ L of a 1 mM solution (THF:Mes, TCB) of the molecular solution into the STM-BJ liquid cell.

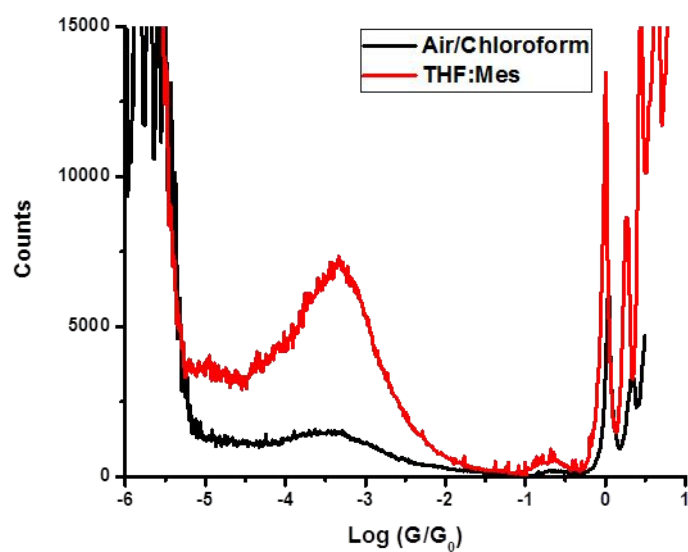


Figure S32: Conductance histogram of **11** in air/chloroform and THF:Mes showing the peak.

Figure S32 shows the improvement of using a solvent mixture THF:Mes for conductance measurements instead of pre-adsorbing the molecule on the surface and carrying out the measurements under air condition.

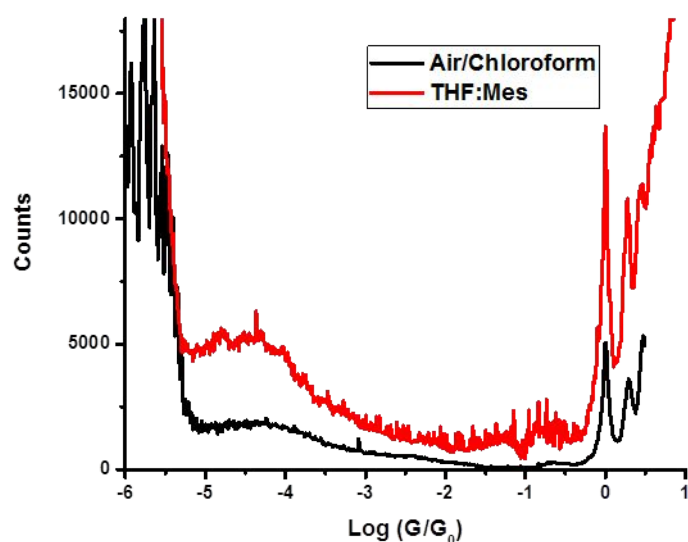


Figure S33: Conductance histogram of **13** in air/chloroform and THF:Mes showing the peak.

Figure S33 shows same improvement for **13** as shown previously for **11**.

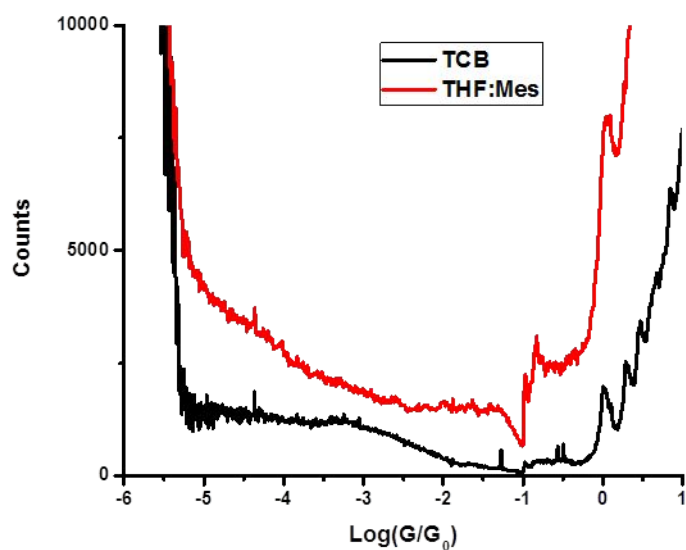


Figure S34: Conductance histogram of **12** in TCB and THF:Mes showing no peak.

Figure S34 shows no molecular junctions between gold electrodes for **12** in any of the two solvents used, the short G_0 peak indicating the gold atomic contact in the 1D-histograms could be read as a hindering effect of the adsorbed molecules on the gold surface inhibiting the gold-gold atomic contact formation.

The compounds differ in molecular length and in number of contact groups respectively.

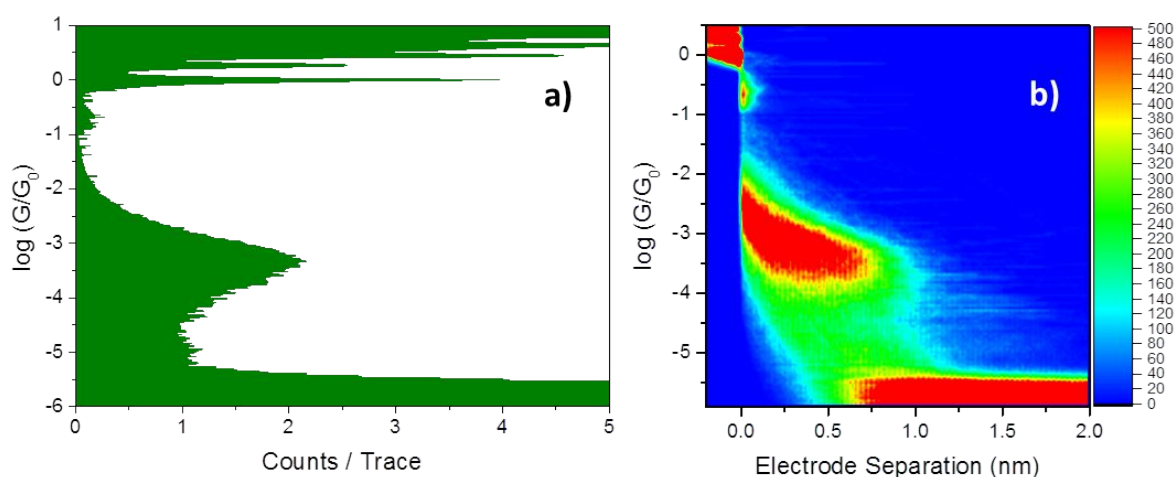


Figure S35: **a)** Break-Junction conductance histograms **11** in air constructed from 3396 measured traces. **b)** 2D-BJ conductance-electrode separation density plot of test molecule in air constructed from 3396 measured traces.

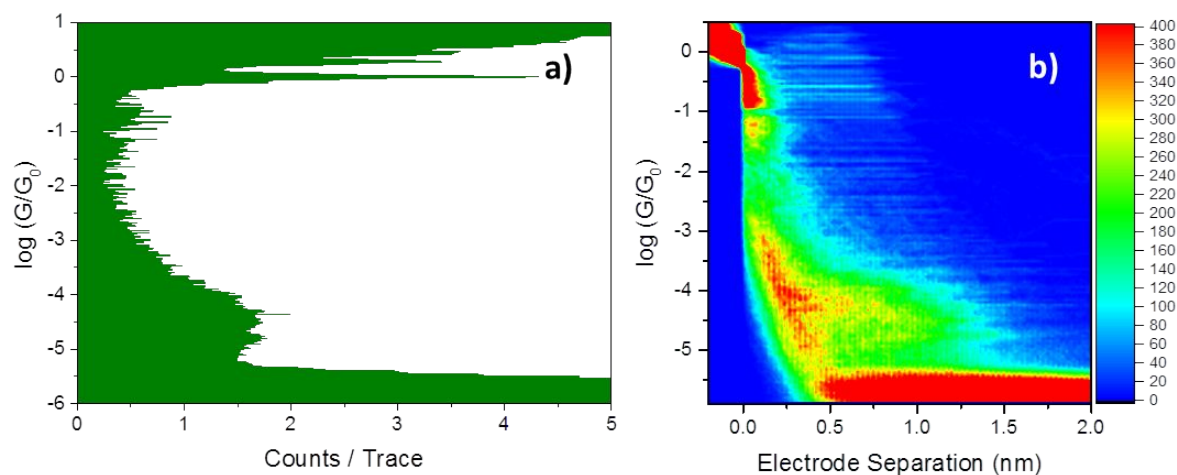


Figure S36: **a)** Break-Junction conductance histograms **13** in air constructed from 3171 measured traces. **b)** 2D-BJ conductance-electrode separation density plot of test molecule in air constructed from 3171 measured traces.

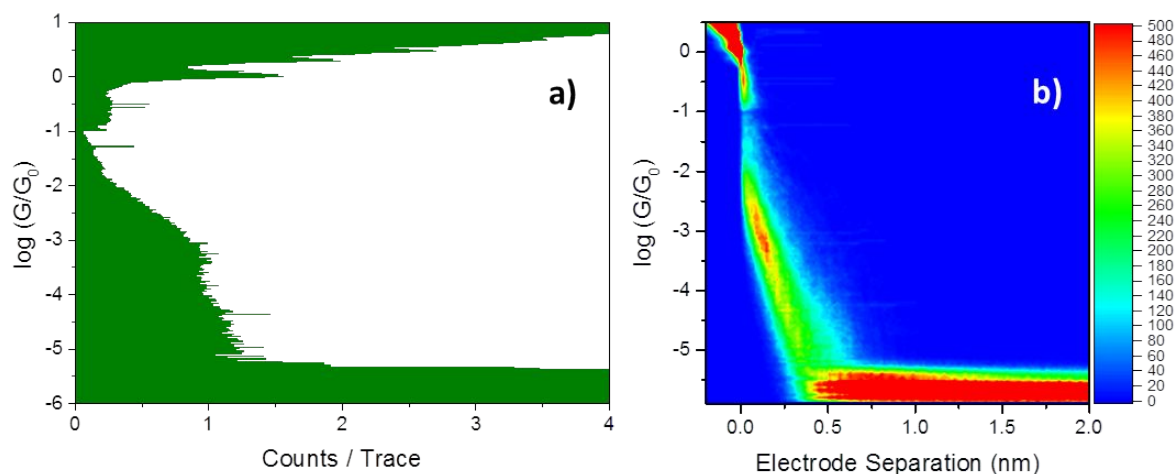


Figure S37: **a)** Break-Junction conductance histograms **12** in air constructed from 3272 measured traces. **b)** 2D-BJ conductance-electrode separation density plot of test molecule in air constructed from 3272 measured traces.

d) Theoretical details

1. Geometry of isolated molecules and their junctions

The DFT code (SIESTA)¹¹ was used to obtain fully relaxed geometries of the isolated molecules, as shown in Figure S38.

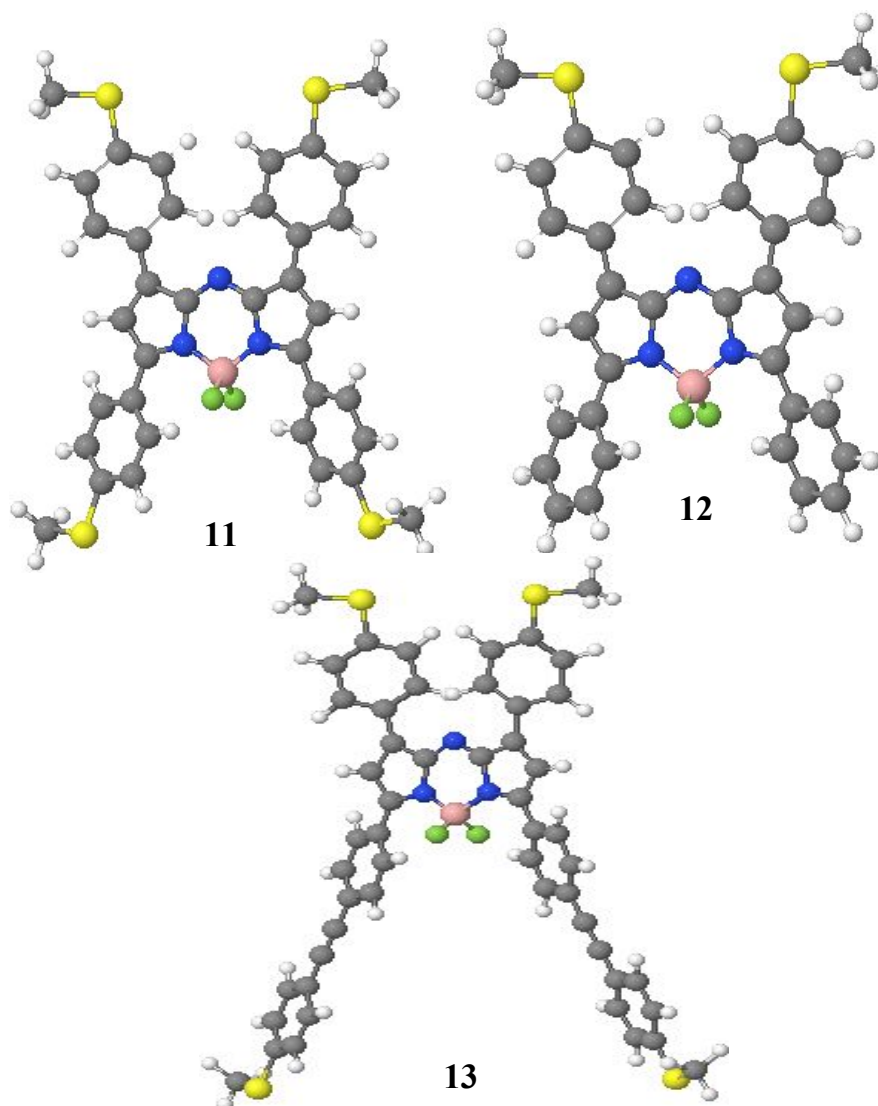


Figure S38. Fully relaxed isolated molecules **11**, **12** and **13** (non-planar molecules)

Then the **11** was connected to gold electrodes in four different geometries as shown in Figure 4 and then further relaxed, similar geometries apply for **13**.

2. Binding energy of 12 on gold via two different anchor groups

We have calculated the binding energy the ‘relaxed’ complex **12** when situated above the gold electrode at various locations. To obtain the results in Figure S39, we moved **12** in 3 dimensions to 252 different positions; along the x-direction it was moved up to 5Å from equilibrium, in the y-direction 10Å and in the z-direction 6Å.

Figure S39 (black curve) shows that when H atoms are placed close to the gold surface as anchor groups, there is only a shallow global minimum. We repeat the same procedure with the SMe anchor group closest to the gold surface Figure S39 (red curve) shows that the energy minimum is much deeper. This shows that **12** does not bind to Au electrode through H atoms, which explains why in our experiments, **12** does not form a junction.

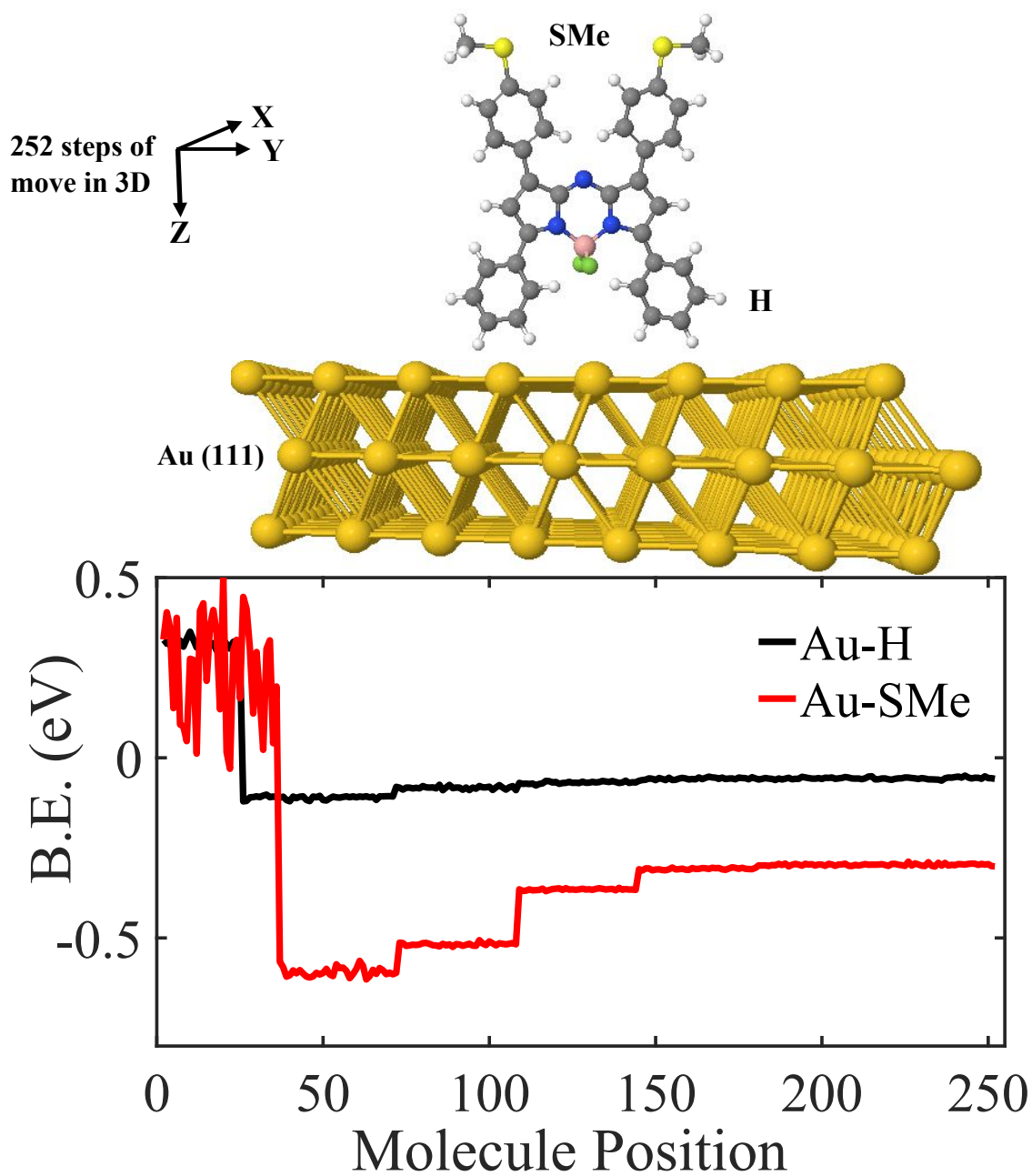


Figure S39: **Top panel:** Orientation of **12** with respect to gold electrode via H atoms anchor. **Lower panel:** Binding energy of **12** to gold electrode as a function of position via two different anchor groups (H and SMe).

3. Do **11** and **13** π -stack onto gold?

To check whether these molecules π -stack onto gold, the lower panel of Figure S40 shows the binding energy of a π -stacked **11** is approximately 0.2 eV (blue curve), whereas the binding energy via the SMe anchor is approximately 0.6 eV (red curve). These show that π -stacking is the least favorable binding motifs. Similar results find for **13** as shown in Figure S41.

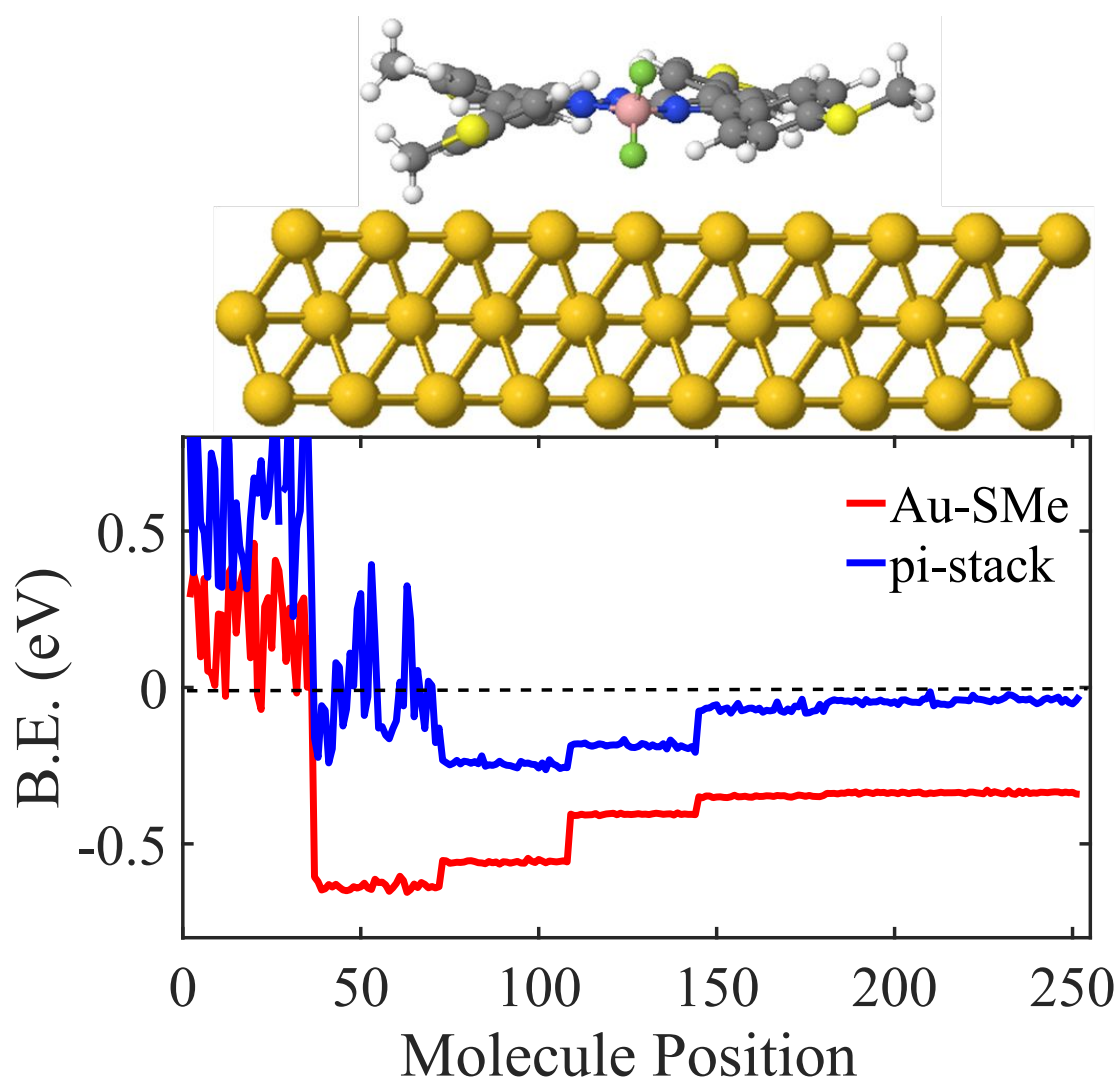


Figure S40: Top panel: Orientation of **11** with respect to gold (π -stacking). Lower panel: Binding energy of **11** π stack onto gold electrode as a function of position in 3 dimensions (blue curve) compared to SMe binding energy.

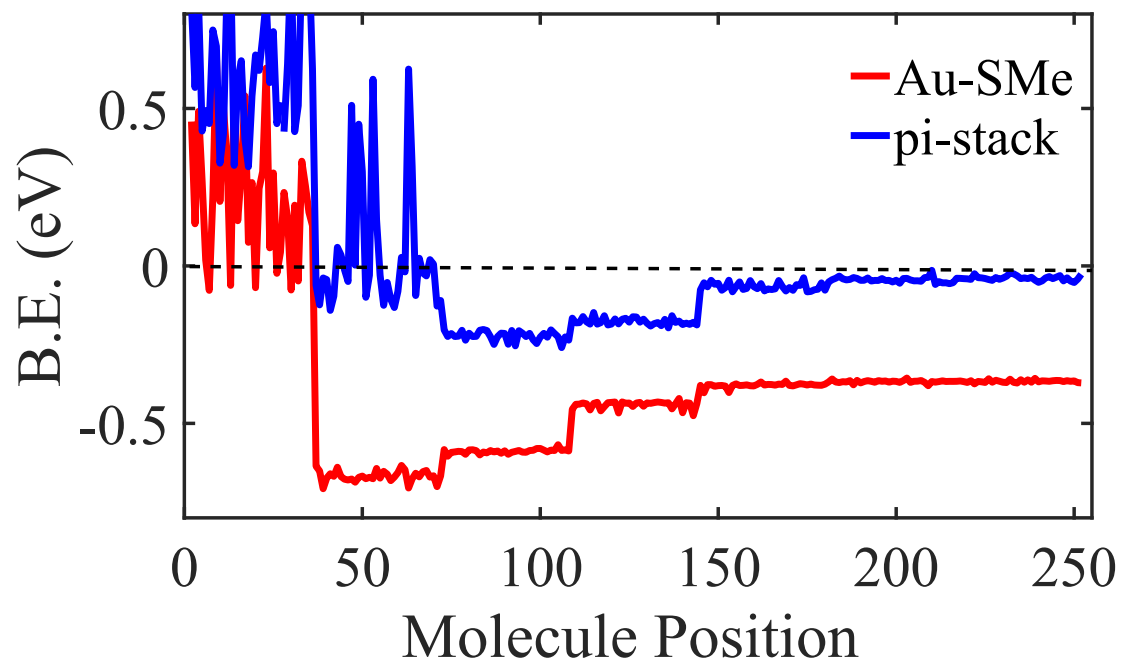


Figure S41: Binding energy of **13** pi stack onto gold electrode as a function of position in 3 dimensions (blue curve) compared to SMe binding energy.

4. Wave function plots for 11, 12 and 13

The plots below show isosurfaces of the HOMO, LUMO, HOMO-1 and LUMO+1 of isolated molecules, along with their energies.

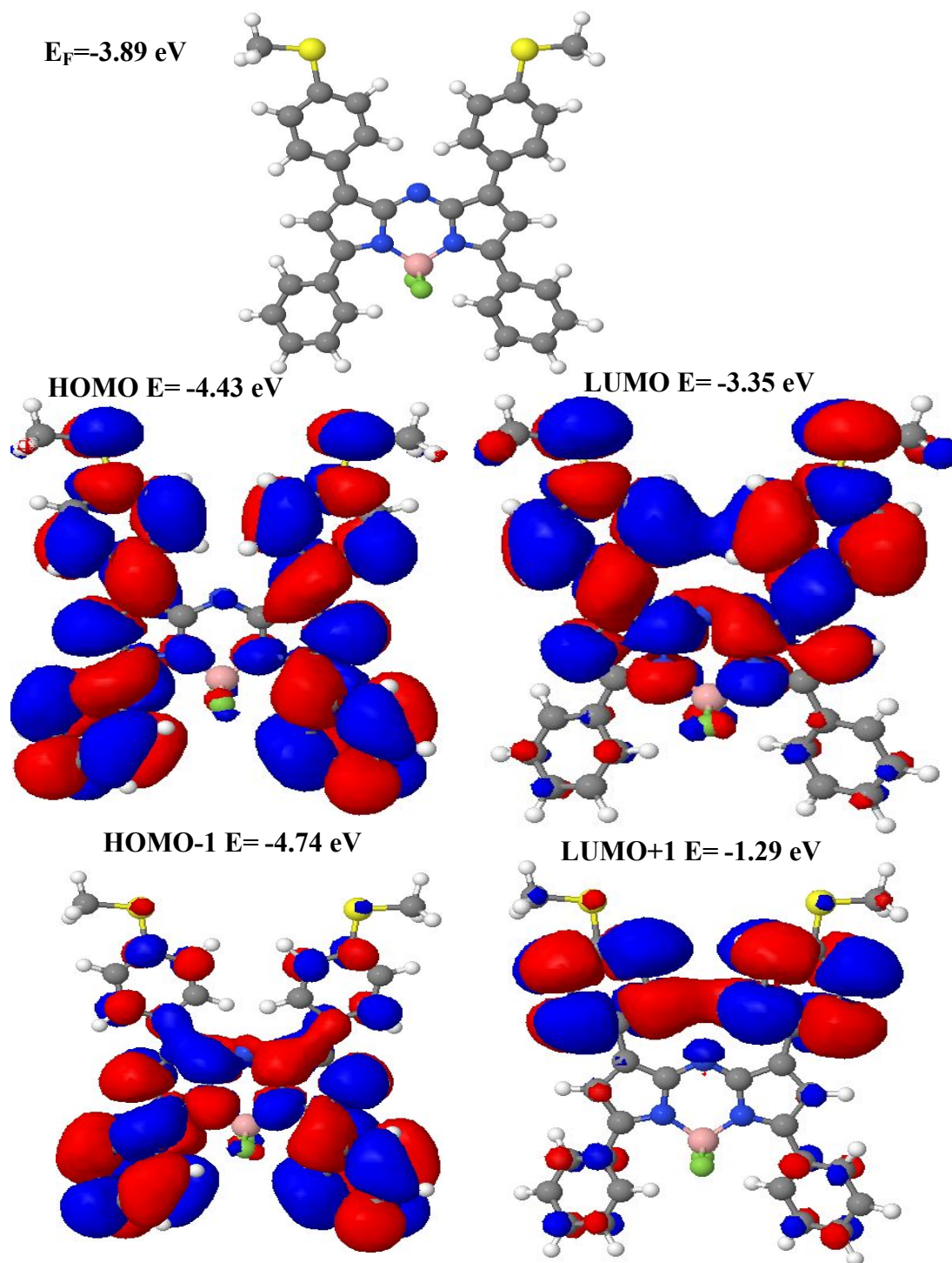


Figure S42. Wave function for 12. **Top panel:** Fully optimised geometry of 12. **Lower panel:** HOMO, LUMO, HOMO-1 and LUMO+1 along with their energies

Figure S42 shows no weight on the both lower rings (H atoms anchor), for both LUMO and LUMO+1, whereas Figure S43 shows a weight on the (S atoms) for HOMO and LUMO plots. This weight clearly supports the binding energy curves, which suggests that this molecule does not bind to Au electrode through the H anchors.

To emphasize that the weight on the anchor group correlates with the anchor binding energy to the electrode, here we plot the wave function for other two molecules (**11** and **13**). In contrast with the right-hand plots of Figure S42, Figures S43 and S44 show a significant HOMO and LUMO weight on the lower end groups of the molecule.

$E_F = -3.61$ eV

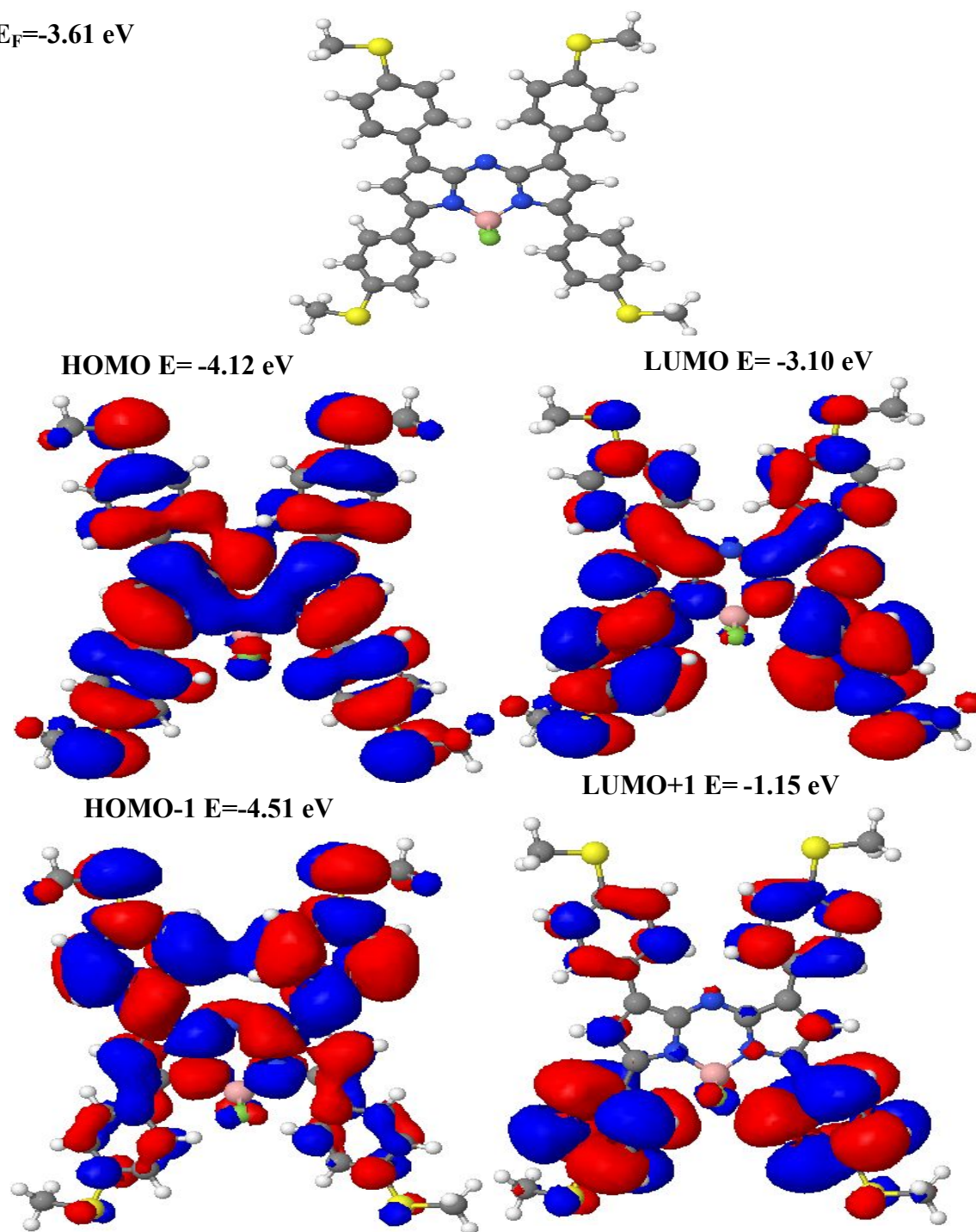
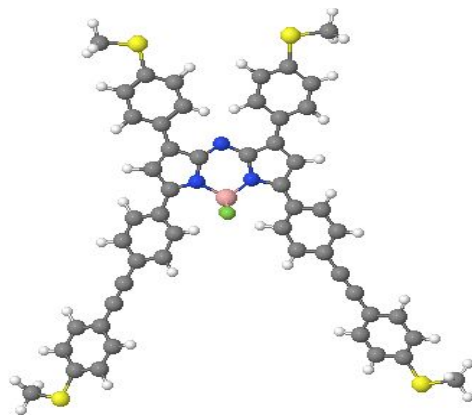
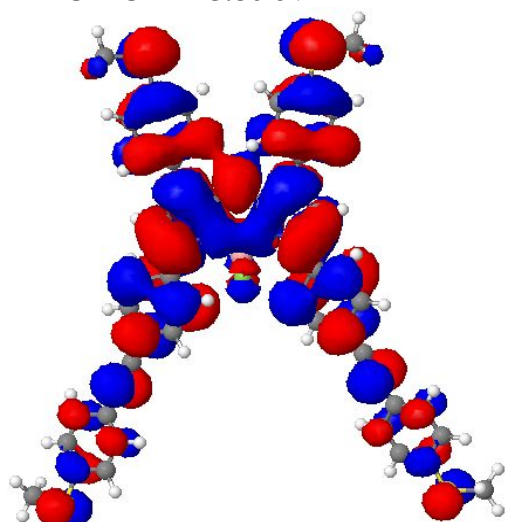


Figure S43. Wave function for **11**. **Top panel:** Fully optimised geometry of **11**. **Lower panel:** HOMO, LUMO, HOMO-1 and LUMO+1 along with their energies

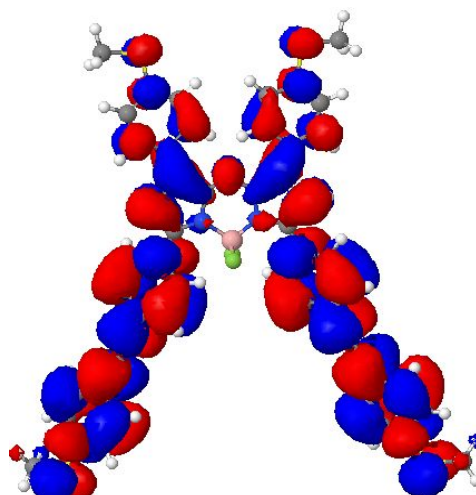
$E_F = -5.40$ eV



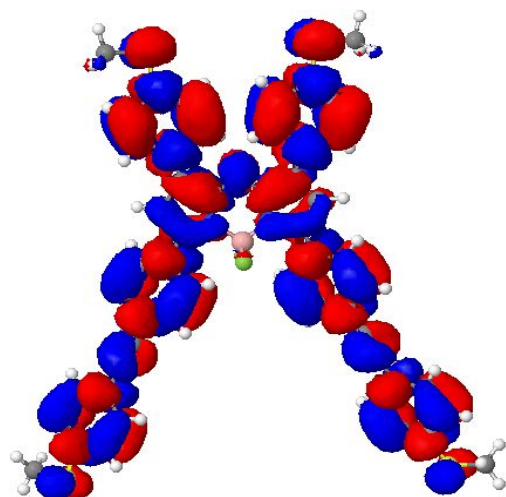
HOMO $E = -5.86$ eV



LUMO $E = -4.94$ eV



HOMO-1 $E = -6.02$ eV



LUMO+1 $E = -3.52$ eV

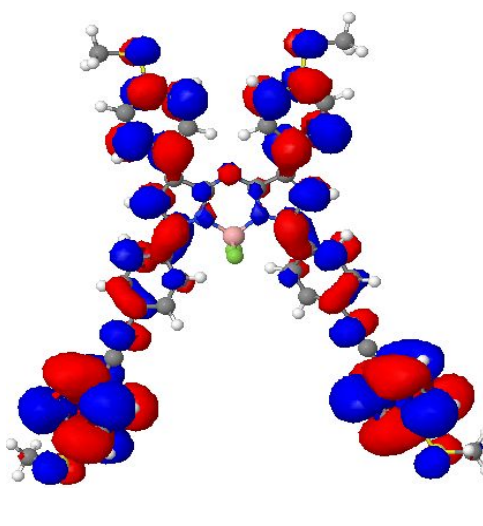


Figure S44. Wave function for **13**. **Top panel:** Fully optimised geometry of **13**. **Lower panel:** HOMO, LUMO, HOMO-1 and LUMO+1 along with their energies

5. HOMO-LUMO gap

HOMO-LUMO gaps have been measured and calculated for **11**, **12** and **13** as shown in Table S16. Theoretical gaps were calculated for isolated molecules and when the molecules are in the junctions, the gap between their HOMO and LUMO transmission resonances are quoted. As shown by the third and fourth columns in Table S16, isolated gaps are usually bigger than the gaps between the transmission resonances this is due to the latter are shifted by the real part of the self-energy of the contact to the leads. To obtain a more accurate HOMO-LUMO gap, we use a scissor correction as described in the main text. Polarization effects can introduce a further correction. However, to our best knowledge there is no reliable way of implementing these image charge effects for the complex molecules considered here. Therefore the HOMO-LUMO gap generated by our scissor correction can be considered to be an upper bound¹².

Table S16: Experimental measurements and theoretical calculations of HOMO–LUMO gaps in (eV) of **11, **12** and **13****

Molecule	^a E _g (Exp.)	^b E _{g, DFT} (Iso.)	^c E _{g, DFT} (Au-M-Au)	Corrected gaps
11	1.74	1.02	0.9	1.70
12	1.85	1.08	<i>No junction</i>	<i>No junction</i>
13	1.74	0.92	0.8	1.80

^aE_g = 1240/λ_{onset UV}. ^bTheoretical HOMO–LUMO band gaps for isolated molecule.

^cTheoretical gaps between HOMO–LUMO transmission resonances.

6. Transmission coefficient

In this section, the transmission coefficient $T(E)$, is calculated for the molecules **11** and **13**. $T(E)$ is calculated for four possible geometries as shown in Figure 4. Figure S45 (left panel) shows that the conductance for **1** exhibits destructive interference (red solid-line), whereas for **2**, **3** and **4** a high conductance. Similarly, when the two anchors participate in conveying electrons, a high conductance prevails and the conductance is slightly higher (comparing the blue line with the black line). Finally, the green solid line shows the transmission coefficient when there are three anchors (geometry 4). These results are obtained without scissor corrections

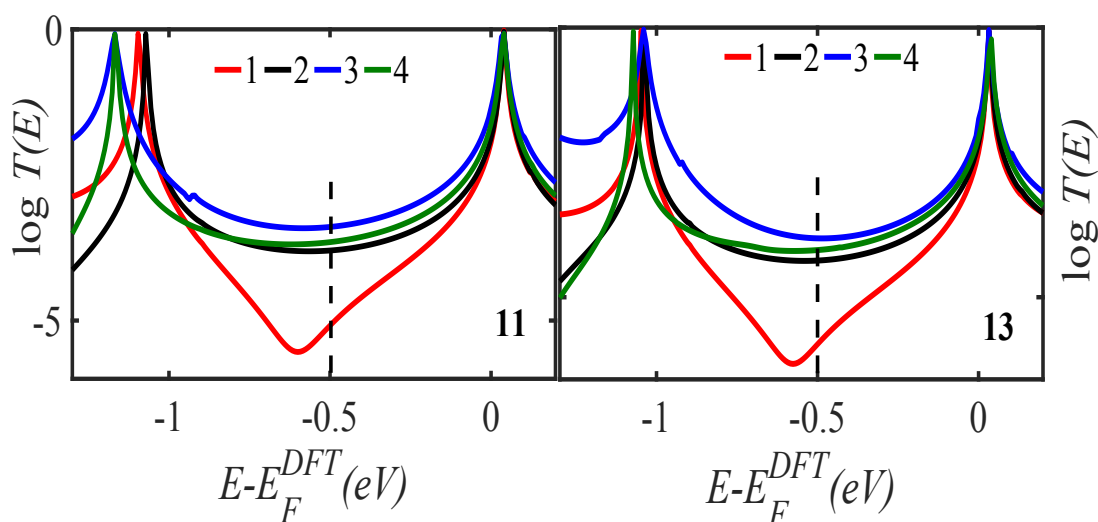


Figure S45: Transmission coefficients $T(E)$ of **11** and **13** in four different possible geometries before scissor corrections (see Figure 4). 1 (red-line), 2 (black-line), 3 (blue-line) and 4 (green-line)

The same calculations were repeated using scissor correction described in the main text, leading to the results shown in Figure S46

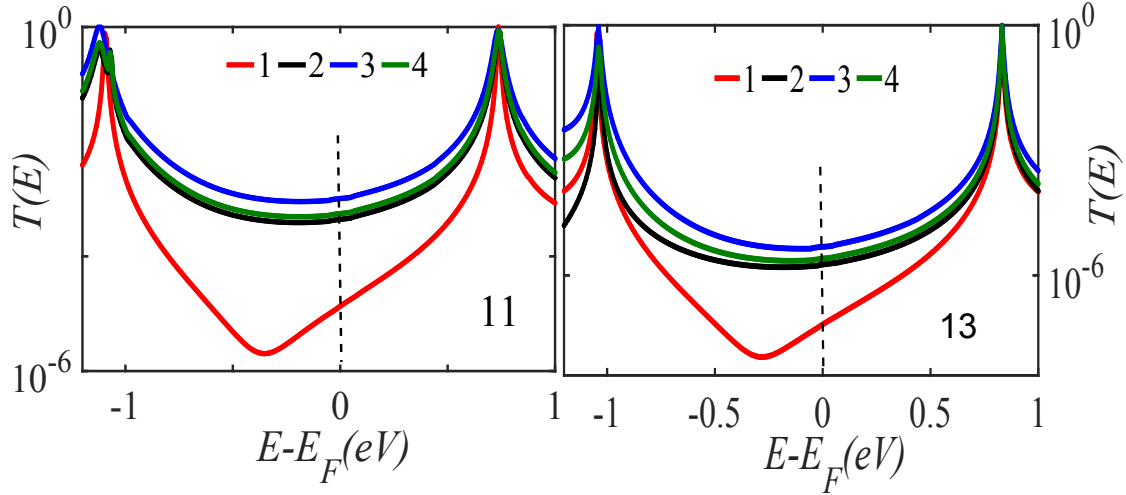


Figure S46: Transmission coefficients $T(E)$ of **11** and **13** in four different possible geometries (see Figure 4). 1 (red-line), 2 (black-line), 3 (blue-line) and 4 (green-line), using scissor correction.

7. Comparison with experimental measurements

The next step is to make a comparison between theoretical calculations and experimental measurements. We believe that the four possible junctions (see Figures 4), are the most favorable geometries to form a junction in the STM. Based on that, we take the average conductance G of geometries 1, 2, 3 and 4 for both **11** and **13** by applying the Landauer formula on the transmission coefficient curves. Figure S47 shows the average conductance curves of **11** and **13**.

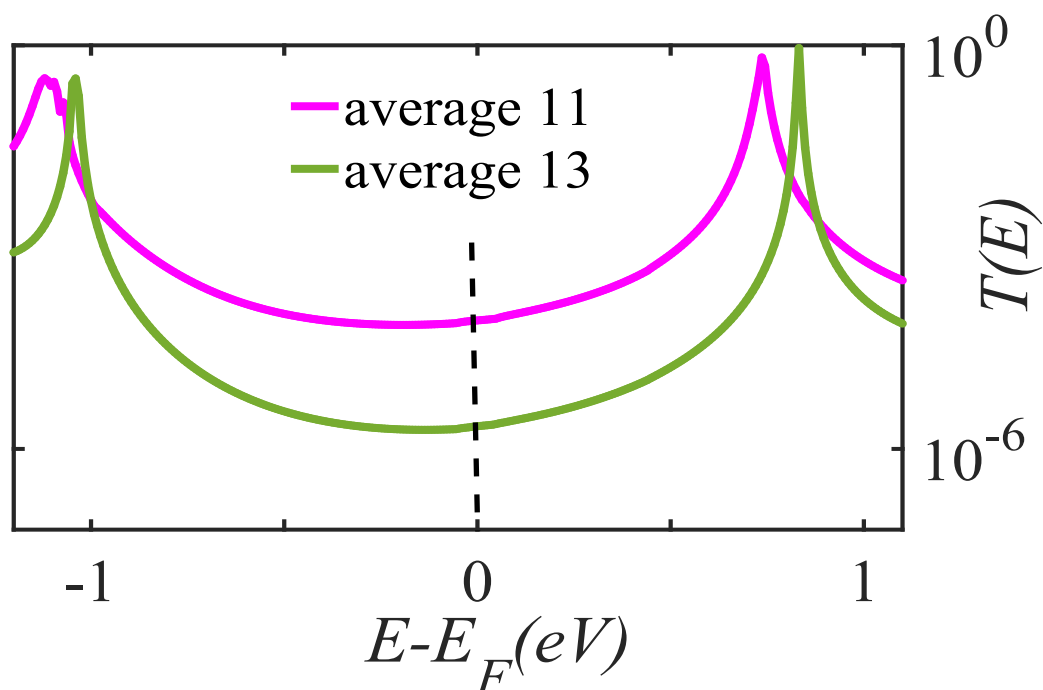


Figure S47: Average conductance G of **11** and **13** in the most favorable geometries. The average curves of **11** and **13** using scissor correction (pink and green respectively)

Table 4 in the main text shows an excellent comparison between the average conductance of the theory and experiment measurements of solutions including mesitylene and air. In this study, we using three molecules **11**, **12** and **13**. It is worth mentioning that **12** molecules experimentally do not form a junction between STM drain and source. Similarly, binding energy calculations indict that **12** does not binding to gold electrode through H atoms anchor. The average theory is taken at $E - E_F^{\text{DFT}} = -0.5$ eV (mid gap).

8. Breaking off distance

Here we compare the breaking off distance with the molecular length. Table S17 shows there is a slight difference between the breaking of distance and the molecular length. For instance, for **11** the molecular length is 1.60 nm whereas the breaking of distance is 1.4 nm in THF/Mesitylene. The difference even smaller for **13**.

Table S17. Break-off distances and molecular length of **11** and **13**

Molecule	Break-Off distance (nm) Exp.		Molecular length (nm) Theo.
	THF/Mesitylene	CHCl ₃ /Air	
11	1.40		1.60
13	1.60		1.70

9. Discussion of alternative binding motifs

In addition to the binding configurations discussed in the main text, we also computed the conductance between both thioanisoles, because it is of interest to determine if conductance between the thioanisoles of **12** would yield a measurable conductance. Figure S48 the transmission coefficient for such a connectivity and confirms that even if the Fermi energy located in the middle of the HOMO-LUMO gap, the conductance would be measurable. Therefore, we conclude that this connectivity is not accessed within our experiments, presumably due to steric hindrance.

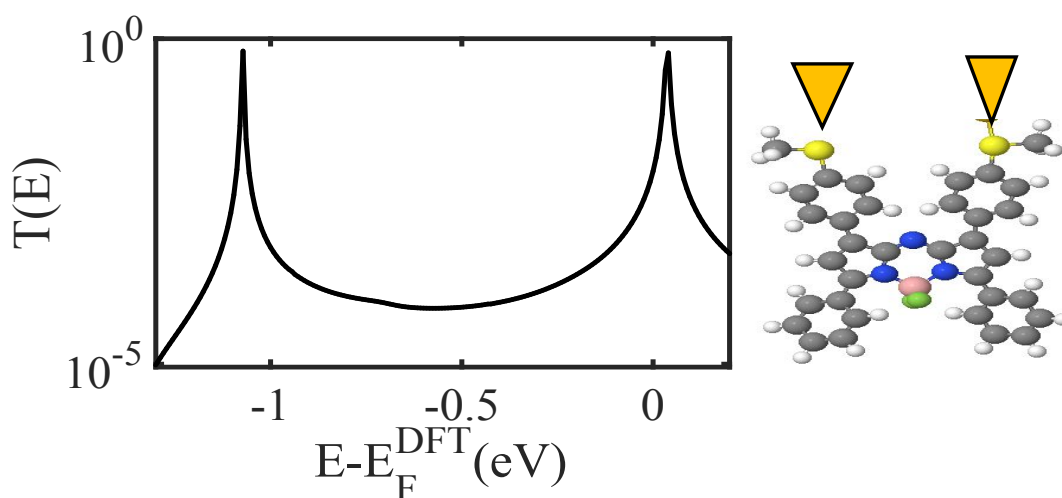


Figure S48: Transmission coefficient $T(E)$ of **12** between both distal thioanisoles (left). The alternative geometry (right)

10. Tight binding model

In what follows, we construct a simple tight binding (i.e. Hückel) Hamiltonian, which describes the connectivity dependence of the electrical conductance of the tetraphenyl-aza-BODIPY central unit. The Hamiltonian matrix consists of diagonal elements $H_{jj} = \epsilon_j$, which describe the

energy ϵ_j of an electron on site j and nearest neighbor off-diagonal elements H_{ij} , which describe hopping integrals between neighboring sites i and j . All other matrix elements are set to zero.

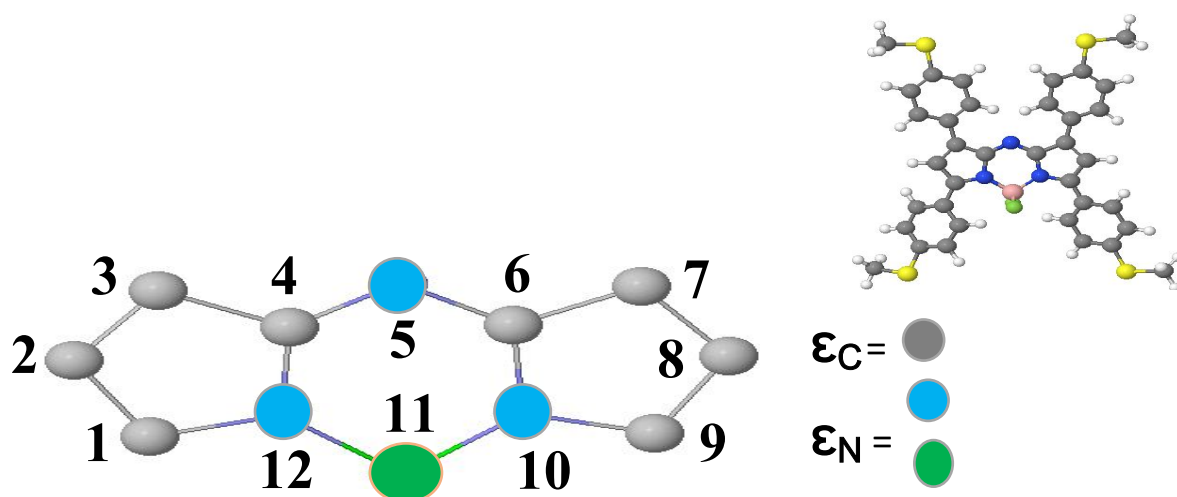


Figure S49 : Lattice representation of the tetraphenyl-aza-BODIPY central unit.

If all the sites were identical, then the simplest model would be obtained by setting all $\epsilon_j=0$ (which defines the zero of energy) and all nearest neighbor couplings equal to -1, which sets the energy scale. Such a Hamiltonian is a simple connectivity table, whose entries H_{ij} are equal to -1 when two atoms i and j are neighbors and are zero otherwise. Despite its simplicity, such a model is found to describe the connectivity dependence of the electrical conductance of molecules with polyaromatic hydrocarbon cores.¹³⁻¹⁴ In our case, there are several inequivalent atoms, colored light blue (nitrogens), dark green (boron) and grey (carbons) in figure S49, and therefore we shall allow ourselves the flexibility of assigning these different site energies, denoted ϵ_C , ϵ_N , ϵ_B , respectively ($\epsilon_C=\epsilon_N=\epsilon_B=0$). In what follows, the hopping integrals are denoted $-\gamma$.

When one-dimensional tight-binding leads are connected to sites 1 and 3, the resulting transmission coefficient is shown as the red curve in figure S50, which clearly exhibits a DQI dip. In contrast, when such leads are connected to sites 1 and 7, the black curve is obtained, which contains no such dip. These results are in qualitative agreement with the transmission plots in Figure 5 of the main text, which show that in the presence of the 1-7 connectivity, there is no DQI dip.

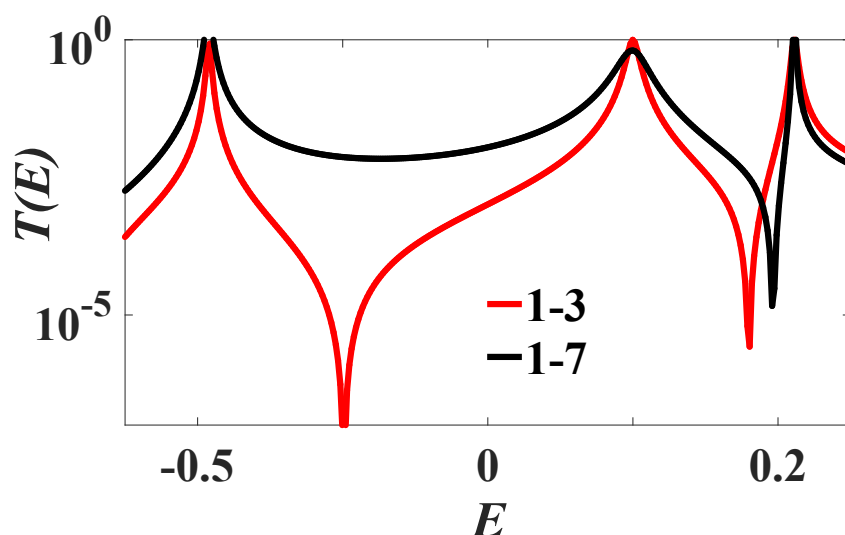


Figure S50: The core transmission coefficient, obtained from the tight binding model when $\gamma=-1$ and $\epsilon_C=\epsilon_N=\epsilon_B=0$, (diagonal (1-7) red-line and straight (1-3) black-line)

e) References

1. Loibl, A.; de Krom, I.; Pidko, E. A.; Weber, M.; Wiecko, J.; Müller, C., Tuning the Electronic Effects of Aromatic Phosphorus Heterocycles: An Unprecedented Phosphinine with Significant P(II)-Donor Properties. *Chemical Communications* **2014**, *50*, 8842-8844.
2. Arakawa, Y.; Kang, S.; Tsuji, H.; Watanabe, J.; Konishi, G.-i., The Design of Liquid Crystalline Bistolane-Based Materials with Extremely High Birefringence. *RSC Advances* **2016**, *6*, 92845-92851.
3. Dolomanov, O. V.; Bourhis, L. J.; Gildea, R. J.; Howard, J. A. K.; Puschmann, H., Olex2: A Complete Structure Solution, Refinement and Analysis Program. *J. Appl. Crystallogr.* **2009**, *42*, 339-341.
4. Sheldrick, G. M. *Shelxl: Suite of Programs for Crystal Structure Analysis*, Tammanstrasse 4: Gottingen, 1998.
5. Davidson, R.; Hsu, Y.; Batchelor, T.; Yufit, D.; Beeby, A., The Use of Organolithium Reagents for the Synthesis of 4-Aryl-2-Phenylpyridines and Their Corresponding Iridium(III) Complexes. *Dalton Trans.* **2016**, *45*, 11496-11507.

6. Bessette, A.; Ferreira, J. G.; Giguère, M.; Bélanger, F.; Désilets, D.; Hanan, G. S., Azadipyrromethene Dye Derivatives in Coordination Chemistry: The Structure–Property Relationship in Homoleptic Metal(II) Complexes. *Inorganic Chemistry* **2012**, *51*, 12132-12141.
7. M. J. Frisch, et al. *Gaussian 09*, A.1; Gaussian, Inc: Wallingford CT, 2009.
8. Dennington, R.; Keith, T.; Millam, J. *Gaussview*, Version 5; Semichem Inc.: Shawnee Mission KS, 2009.
9. O'Boyle, N. M.; Tenderholt, A. L.; Langner, K. M., Cclib: A Library for Package-Independent Computational Chemistry Algorithms. *J. Comput. Chem.* **2008**, *29*, 839-845.
10. Haiss, W.; Lackey, D.; Sass, J. K.; Besocke, K. H., Atomic Resolution Scanning Tunneling Microscopy Images of Au(111) Surfaces in Air and Polar Organic Solvents. *J. Chem. Phys.* **1991**, *95*, 2193-2196.
11. Soler, J. M.; Artacho, E.; Gale, J. D.; García, A.; Junquera, J.; Ordejón, P.; Sánchez-Portal, D., The Siesta Method for Ab Initio Order-N Materials Simulation. *J. Phys. Condes. Matter* **2002**, *14*, 2745-2779.
12. Quek, Su Ying, Latha Venkataraman, Hyoung Joon Choi, Steven G. Louie, Mark S. Hybertsen, and J. B. Neaton. "Amine– gold linked single-molecule circuits: experiment and theory." *Nano Letters* **2007**, *7*, 11, 3477-3482.
13. Geng, Y.; Sangtarash, S.; Huang, C.; Sadeghi, H.; Fu, Y.; Hong, W.; Wandlowski, T.; Decurtins, S.; Lambert, C. J.; Liu, S.-X., Magic Ratios for Connectivity-Driven Electrical Conductance of Graphene-Like Molecules. *Journal of the American Chemical Society* **2015**, *137*, 4469-4476.
14. Lambert, C. J., Basic Concepts of Quantum Interference and Electron Transport in Single-Molecule Electronics. *Chem. Soc. Rev.* **2015**, *44*, 875-888.